BIG – Branschsamverkan i grunden

Forskningsprogram för effektiv och säker grundläggning av vägar och järnvägar

Projekt A2016:05

Modelling deformations below high-speed rail

Final report from project

CHALMERS UNIVERSITY OF TECHNOLOGY

KTH

TRAFIKVERKET

STATENS GEOTEKNISKA INSTITUT

LULEÅ TEKNISKA UNIVERSITET

BIG – Branschsamverkan i grunden

Forskningsprogram för effektiv och säker grundläggning av vägar och järnvägar

Rapport BIG projekt A2016:05

Modelling deformations below high-speed rail

Final report from project

Jelke Dijkstra and Hossein Tahershamsi

CHALMERS

Framtagen inom ramen för BIG av Chalmers tekniska högskola

Göteborg 2020

Rapport publicerad av BIG, Branschsamverkan i grunden
Beställning Web: www.big-geo.se

ISBN 978-91-986926-3-1
Upplaga Digital

Framtagen av Chalmers Tekniska Högskola
Department of Achetecture &Civil Engineering
Geology & Geotechnics
Författare Jelke Dijkstra, Hossein Tahershamsi



CHALMERS

Modelling deformations below high-speed rail

JELKE DIJKSTRA & HOSSEIN TAHERSHAMSI

Department of Architecture and Civil Engineering
Geology & Geotechnics
CHALMERS UNIVERSITY OF TECHNOLOGY
Göteborg, Sweden 2020

TECHNICAL REPORT GEOTECHNICAL ENGINEERING

Modelling deformations below high-speed rail

JELKE DIJKSTRA & HOSSEIN TAHERSHAMSI

Department of Architecture and Civil Engineering
Geology & Geotechnics
CHALMERS UNIVERSITY OF TECHNOLOGY
Göteborg, Sweden 2020

Modelling deformations below high-speed rail
JELKE DIJKSTRA & HOSSEIN TAHERSHAMSI
ISBN xxx

© JELKE DIJKSTRA & HOSSEIN TAHERSHAMSI, 2020

Technical report 2020:APR30
ISSN xxx-xxx
Department of Architecture and Civil Engineering
Geology & Geotechnics
Chalmers University of Technology
SE-412 96 Göteborg
Sweden
Telephone: +46 (0)31-772 2120

Chalmers Reproservice
Göteborg, Sweden 2020

Modelling deformations below high-speed rail
Technical report Geotechnical Engineering
JELKE DIJKSTRA & HOSSEIN TAHERSHAMSI
Department of Architecture and Civil Engineering
Geology & Geotechnics
Chalmers University of Technology

Abstract

In many situations, a previously adequate railway track foundation starts to emit stronger than expected ground vibrations in the soil and the existing vibration mitigating solutions become inadequate. The subsoil is the most persistent source of these issues, as track and subgrade related causes can be addressed during maintenance cycles. Over the lifetime of the structure the dynamic soil properties, especially in weakly bonded soft soils such as those in the Nordic countries, will change under repeated dynamic loading from the traffic. Even for otherwise mechanically stable piled track-slab solutions the dynamic soil properties continue to change with on-going slow processes, such as consolidation and creep in the soft soils. Furthermore, these slow processes themselves (timescale of years) are dependent on the cyclic loading from the tens of thousand trains passing by. The interaction between these two processes is complex and not fully resolved. This report presents a first step towards modelling these complex systems by presenting a numerical methodology that captures both the slow processes via a newly developed strain accumulation model for soft soils and the dynamic response via time-domain based Finite Element analyses. To further study the interdependence of parameter a framework for rigorous sensitivity analyses has been extended for use with boundary value level FE analyses. The constitutive model and all FE analyses and scripts in the calculation are developed for the *Tochnog Professional* code.

The results indicate that the permanent settlements of an embankment on clay increase with increasing axle load (at constant loading period), but reduce with increasing train speed (at constant axle load). The resulting changes in the subsoil, in terms of plastic strain, irreversible degradation of bonds, have potentially profound effects on the subsequent dynamic response of the system. The sensitivity is largest for the loading period with little interdependence between the amplitude and the loading period, which was not expected. The sensitivity results are consistent for all locations below the embankment considered.

The remaining challenge outstanding is a more strong coupling of the link between the damage (or destructuration) parameter χ and the material stiffness, which requires more experimental data. Furthermore, a more systematic sensitivity analysis of the interaction between slow and fast processes in the soil and the effect of track configuration and soil conditions is ongoing in a follow up project. This ultimately will lead to quantification and spatial distribution of the changed properties in the soft soil for several loading scenarios and its impact on the critical train velocities for the railway system above.

The measurable project impact is itemized below:

- New constitutive model for strain accumulation of soft sensitive clay;
- Framework for systematic sensitivity analyses at boundary value level;
- The resulting analysis method is likely to be used to inform future recommendations for Geostructures as part of Östlånken;

- All calculations can be performed with the *Tochnog Professional* Finite Element code, which since January 2020 is free to use for all. This dramatically improves market adaptation.

Keywords: strain accumulation, time effects, high-speed rail, soft soils, sensitivity analyses

Contents

Abstract **i**

Contents **iii**

1 Introduction **1**
1.1 Background . . . 1
1.2 Aim . . . 2
1.3 Objectives . . . 2
1.4 Limitations . . . 2

2 Methodology **3**
2.1 Introduction . . . 3
2.2 Static, quasi-static and dynamic modelling of soils using FE . . . 3
2.2.1 Principal differences . . . 3
2.2.2 Dynamic modelling using FEM . . . 3
2.2.3 Effective stress models . . . 5
2.2.4 Final message . . . 5
2.3 Adding strain accumulation to Creep-Sclay1s . . . 5
2.3.1 Experimental evidence . . . 5
2.3.2 Original model for soft soils . . . 6
2.3.3 Model concept for strain accumulation . . . 6
2.3.4 Strain accumulation extension for Creep-Sclay1s . . . 7
2.4 Sensitivity analyses . . . 8
2.4.1 Principles . . . 8
2.4.2 Single integration point . . . 9
2.4.3 Multi-element level . . . 10

3 Strain accumulation below high-speed rail **12**
3.1 Introduction . . . 12
3.2 Embankment on soft soil . . . 12
3.2.1 Numerical model . . . 12
3.2.2 Results reference calculations . . . 14
3.3 Sensitivity analyses . . . 15
3.3.1 Scenarios . . . 15
3.3.2 Results . . . 15

4 Conclusions & Recommendations **18**
4.1 Conclusions . . . 18
4.2 Recommendations . . . 18

References **19**

1 Introduction

1.1 Background

Problem origin

In many situations, a previously adequate railway track foundation progressively starts to emit stronger than expected low frequency ground vibrations in the soil and the existing vibration mitigating solutions become inadequate. In addition permanent settlements of the rail head accumulate. The subsoil is the most persistent source of these track degradation issues over the lifetime of the structure, as track and subgrade related causes can be addressed during maintenance cycles. A further indicator of the importance of the subsoil is that the design of most railway tracks is largely similar for the majority of tracks in Europe, yet large differences in observed settlements are observed. With increasing train velocities the demands for the track-alignment, its dynamic response and the allowable tolerances over time become more stringent. Yet, technical solutions that meet those demands should be cost-effective and robust over time, even when the subsoil and its dynamic soil properties are slowly evolving during track operation.

Traditional modelling strategies

Most rail track-bed modelling strategies only consider the dynamic response of the track-ballast and subgrade without incorporating the response of the deeper soil layers, also totally ignoring effects of groundwater. Therefore, slow processes that affect the dynamic response of the subsoil, such as generation and dissipation of pore pressures and creep that are accelerated under quasi-static and dynamic loading, (e.g., Coelho et al. 2011) are totally ignored. Typically, the pores in the soil are completely saturated with water, affecting the wave propagation, which essentially occurs as a single pressure wave and shear wave.

Often the soil behaviour is approximated with linear elastic models to study wave propagation and dynamic track response using Finite Element (FE), Boundary Element Method (BE) method or mixed BE/FE (Lombeart et al. 2006; Madshus and Kaynia 2000). The focus has been on a single train passage, and the associated dynamic track response and vibrations propagating through the environment, most notably critical track velocities (e.g., Adolfsson et al. 1999). Most soil response under a dynamically loaded track can be considered quasi-static, and can therefore be analysed using ordinary dynamic FE methods without explicitly modelling the train. This allows incorporation of more advanced constitutive models for the soil, such as those developed at Chalmers for sensitive clays.

For noise and vibration analysis the soil can be modelled as an equivalent elastic medium, provided that the density and incompressibility of the saturated soil layers are accounted for by equivalent Lamé coefficients (Schevenels et al. 2004). These elastic properties, however will evolve due the slow changing processes in the soil properties from the many train passages.

It is impossible to simulate every train passage in full detail, in order to predict the slow changing processes in the subsoil resulting from quasi-static loading. An attractive approach is to model the effects of many passages using a strain accumulation model.

Strain accumulation models for ballast and soils

When complex constitutive models, specifically designed to truthfully capture each loading cycle (e.g. those inspired by the work of Mrŏz et al. 1978), are used to solve cyclic problems with a large number of loading cycles, $O(10^5)$, issues related to the computational cost and numerical convergence arise. In order to overcome these difficulties, several authors have developed cumulative degradation models to account for the effects of cyclic plastic strains of a large number of loading cycles (Karg et al. 2010; Li et al. 2016; Ni et al. 2014; Niemunis et al. 2005; Pasten et al. 2014; Suiker and Borst 2003). With exception of the work of Ni et al. (2014), all the existing models were developed for coarse grained granular materials. Therefore, there is a lack of models suitable for simulating soft soils. The main limitation of the model presented by Ni et al. (2014) is that it ignores fundamental soft soil features, such as rate-dependency, anisotropy and degradation of bonding (Karstunen et al. 2005; Leroueil and Vaughan 1990; Wheeler et al. 2003). This project aims to address these limitations by developing an accumulation model for soft sensitive clays.

1.2 Aim

A new constitutive model, Creep-Sclay1Sc, will be developed to implicitly capture the effects from cyclic loading of soft soils, by extending the original Creep-Sclay1S model (Sivasithamparam et al. 2015). The aim of this model it to capture the change in clay properties due to long-term cyclic loading with a reasonable accuracy, for subsequent future use in dynamic analyses.

1.3 Objectives

- Development of a constitutive model for cyclic loading of sensitive clay
- Model calibration against a well documented data set on intact natural sensitive clays
- Sensitivity study on the effect of loading period (train velocity) and loading amplitude (or axle load) on the resulting model response

1.4 Limitations

- The study only focuses on quasi-static effects in natural sensitive clays
- Simplified problem geometry without explicitly modelling the foundation structure

2 Methodology

2.1 Introduction

After discussing some basic considerations on modelling dynamic problems using the Finite Element Method, a new strain accumulation model that captures the permanent effects of cyclic loading is proposed and its applicability at boundary value level demonstrated. Subsequently, a rigorous method for sensitivity analyses is introduced for further use in conjunction with the newly proposed model.

The main features of the methods discussed in this Chapter, i.e. the model extension for strain accumulation and the method for sensitivity analysis have been published (or are under review) and are elaborated in more detail in Appendix A & B.

2.2 Static, quasi-static and dynamic modelling of soils using FE

2.2.1 Principal differences

In engineering the differences between static, quasi-static and dynamic loading are not always fully elaborated. A static load does not change over time, examples are the self-weight of a construction. If, on the other hand, the load is changing over time, this change in load has to be considered. Generally, quasi-static loads change sufficiently slow that effects from inertia are negligible, whilst for dynamic loads inertia cannot be ignored. Here, inertia is defined as the resistance (inertial loads) of a physical object to a change of velocity (or its loading direction). Following, the above reasoning a cyclic load can be considered a quasi-static load or a dynamic load depending on the magnitude of the period T (or frequency f) of the load. The faster the load is changing (shorter period, higher frequency) the more likely inertial effects cannot be ignored. In engineering practice this cut-off frequency is somewhat arbitrary chosen. A value for the frequency $f \approx 10\,\mathrm{Hz}$ is not uncommon but lacks a sound scientific base.

The difference between quasi-static loading and dynamic loading is not just governed by the time period over which the change occurs, also the loading amplitude matters. Hence, the definition that the acceleration is $<<$ gravitational acceleration g (i.e. the magnitude of the static load under self weight) is more precise. For a harmonic load with amplitude A and angular frequency $\omega = \frac{2\pi}{T} = 2\pi f$ one can demonstrate that in case the product $A\omega^2 << g$ the load can be considered quasi-static.

In the current report the train loads associated with a single train passage are considered dynamic, whilst the cumulative effect of multiple trains passing over the duration of years is considered quasi-static.

2.2.2 Dynamic modelling using FEM

The Finite Element Method is ideally suited for solving Partial Differential Equations for a domain of arbitrary shape, using boundary conditions that vary over time with constitutive models that simulate the evolving soil behaviour. It is not the purpose to reiterate the basic concepts on dynamic modelling using FEM, rather at this stage it is essential to contrast the

differences to regular FE analyses in geotechnics, as well as elaborating that the constitutive model (including the newly proposed model in this research) does not necessarily need any specific considerations. For a full treatise on the topic is referred to the standard works in the domain (e.g. Cook et al. 1989; Hughes 2012).

The material equilibrium equations that govern the dynamic response considered here are derived by requiring the work of external forces to be absorbed by the work of internal (proportional to displacements in the domain $\mathbf{u}$), inertial (proportional to accelerations $\ddot{\mathbf{u}}$), and viscous (proportional to velocity $\dot{\mathbf{u}}$) forces for any small kinematically admissible motion (Cook et al. 1989). In the usual matrix notation used for FE this leads for a single element to:

$$[\mathbf{m}]\{\ddot{\mathbf{d}}\} + [\mathbf{c}]\{\dot{\mathbf{d}}\} + \{\mathbf{r}^{\mathbf{int}}\} = \{\mathbf{r}^{\mathbf{ext}}\} \tag{2.1}$$

Where $\mathbf{d}$ are the nodal degrees of freedom that are only a function of time, as the spatial distribution of the displacement fields $\mathbf{u}$ (and its derivatives) are integrated using shape functions $\mathbf{N}$, i.e.:

$$\{\mathbf{u}\} = [\mathbf{N}]\{\mathbf{d}\}\ \{\dot{\mathbf{u}}\} = [\mathbf{N}]\{\dot{\mathbf{d}}\}\ \{\ddot{\mathbf{u}}\} = [\mathbf{N}]\{\ddot{\mathbf{d}}\} \tag{2.2}$$

The element mass matrix $\mathbf{m}$ and damping matrix $\mathbf{c}$ comprise of the volume integrated quantities (using the shape functions) equivalent to $m = \rho V$ and $c = \kappa_d V$. Where ρ is the density of the material and κ_d the viscous damping. The external load vector $\{\mathbf{r}^{\mathbf{ext}}\}$ come from the neighbouring elements and the boundary conditions (such as loads, fixities, body forces), whereas the internal force vector $\{\mathbf{r}^{\mathbf{int}}\}$ represents the force (resistance) arising from the material deformations (that result from $\{\mathbf{d}\}$) and the constitutive model used. Subsequently, the contribution of each element are assembled in one large system matrix before being solved.

In traditional geotechnical (quasi-) static analyses, when $\{\ddot{\mathbf{d}}\}$ and $\{\dot{\mathbf{d}}\}$ are negligible, only a solution for $\{\mathbf{d}\}$ is sought where $\{\mathbf{r}^{\mathbf{int}}\}$ and $\{\mathbf{r}^{\mathbf{ext}}\}$ are in equilibrium for the instance of time (or load step) considered. In other words there is no inertia or damping considered, all external loads are balanced by the internal forces.

In a dynamic calculation all terms in Equation 2.1 are solved numerically. There are many approaches to achieve this, depending on the exact formulation of the problem and the solution that is needed (modal analysis, stress wave propagation). Linear systems (where the material model is also linear elastic) have particular advantages that allow those to be solved more efficiently. In the current work the problem is highly non-linear due to the constitutive model for the material, as well as the presence of a groundwater, hence the system is solved in the time domain by calculating the state incrementally for each time step. This is computationally expensive, in terms of calculation time, but poses no problems for two-dimensional (2D) problems. Furthermore, the type of time integration and element type (and size) used will influence the accuracy of the solution quite dramatically, however, for most geotechnical problems with low frequency events a general purpose explicit or implicit solver will suffice. It should be noted, however, that as opposed to 3D analyses a 2D analysis will not properly capture the geometric component of the damping (radiation damping) and explicit schemes, whilst more efficient, are not always compatible with the requirements for solving a coupled system of equations (mechanical + hydraulic).

2.2.3 Effective stress models

The internal force vector $\{\mathbf{r}^{\mathbf{int}}\}$ in Equation 2.1 represents the forces arising from the internal material response. In solid mechanics this is mainly the stress resulting from the deformations behaviour in the solid material. In geotechnics this is more complicated, as now the sum of the effective stress component and the porewater pressures contribute to this force vector. The constitutive model proposed here relates the strain increment (deformations) to an increment of effective stress. Depending on the nature of the implementation the pore water pressures are calculated separately or in a coupled fashion where the effective stress and porewater pressures are solved simultaneously using one system of equations. Furthermore, by coupling the deformations of the solid skeleton to the generation of porewater pressures, so called consolidation analysis, the dynamic response of both the solid and the fluid phase is captured adequately.

2.2.4 Final message

As long the Finite Element framework used solves the complete set of equilibrium equation that includes the inertial and viscous terms, adding the dynamic material response in a geotechnical analysis is rather straight forward. The constitutive model for the soil does not need to be adapted for dynamic analyses (as long a global damping matrix suffices) and the excess pore water pressures from dynamic loading are captured as well. Only in extreme cases (large impact loads, high frequency events) or for extreme accuracy more specialist codes should be employed. The latter are often only incorporating linear elastic soil behaviour, hence are inadequate. Some of those codes, however, have an improved approach to capture inertial effects of the pore fluid more accurately, i.e., not just an undrained pore pressure wave (Zienkiewicz and Shiomi 1984). The *Tochnog Professional* FE code adopted in this research has successfully been used for dynamic problems related to railway systems (e.g., Wegener 2013; Zuada Coelho and Hicks 2016).

2.3 Adding strain accumulation to Creep-Sclay1s

2.3.1 Experimental evidence

Currently, only few data sets are available that studies the effect of loading frequency and loading amplitude on the response of natural sensitive clays (Li et al. 2011; Wichtmann et al. 2013). Figure 2.1 shows that the cyclic undrained triaxial tests show three main trends:

- There is a semi-logarithmic relation between the axial strain and the number of cycles (or time), until the onset of failure;
- The number of cycles until failure reduces with increasing cyclic shear stress amplitude A (t_{cy} normalised with the undrained shear strength in compression s_u^c in Figure 2.1);
- The number of cycles until failure reduces with increasing period T (decreasing frequency f in Figure 2.1);

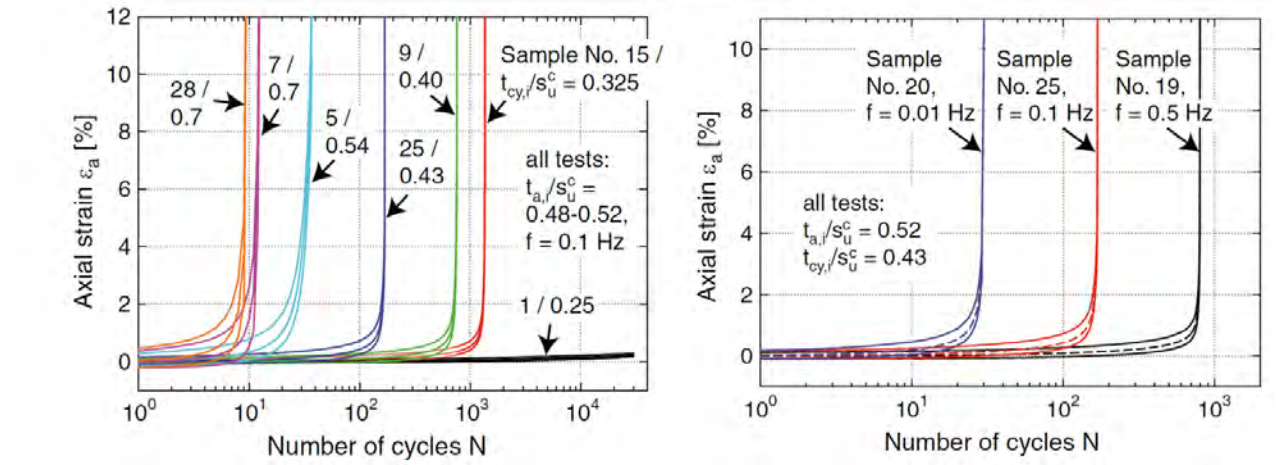


Figure 2.1: *Effect of shear loading amplitude (left) and loading period (right); (Wichtmann et al. 2013)*

2.3.2 Original model for soft soils

Soft sensitive soils have specific features that need to be incorporated in the constitutive model in order to capture the appropriate mechanical response. Here, we follow the work of Karstunen and co-workers who developed the SCLAY1(s) family of models that incorporate anisotropy (strength/stiffness); destructuration (bond degradation) and creep. The rationale and model details have been discussed in length elsewhere (e.g. Wheeler et al. 2003; Karstunen et al. 2005; Sivasithamparam et al. 2015; Gras et al. 2017; Gras et al. 2018). The most complete model is the Creep-Sclay1s model, a 3D effective stress model that is implemented in UMAT form. The UMAT implementations makes the model suitable for the single element strain driver (Niemunis et al. 2005) and the FE code used here (*Tochnog Professional*). A lay-person description of the model is readily found in the Trafikverket BEST report (Karstunen and Amavasai 2017).

In addition to anisotropy and structure, soft clays also exhibit viscous behaviour, such as rate dependency and creep. This additional property incorporates the time dimension in the material description. Creep-Sclay1s is an elasto-viscoplastic constitutive model capable of modelling rate dependency. It is this elasto-viscoplastic formulation that is exploited for the incorporation of strain accumulation effects.

2.3.3 Model concept for strain accumulation

Strain accumulation occurs during a loading cycle (a stress loop) when the corresponding strain loop is not closed. The material is not returning to its original configuration and a permanent irrecoverable strain remains. When this complete loading cycle is modelled using a generalised stress-strain relation as available in most constitutive models, the permanent strain from cyclic loading follows *implicitly*. There is no direct relation between the number of loading cycles (or elapsed time) and the magnitude of the accumulated strain. In contrast, *explicit* models directly relate the properties of the loading cycle to the emerging irrecoverable strain. Figure 2.2 shows the principle of an explicit strain accumulation model clearly. These models are more efficient and robust for the modelling of a large number of loading cycles.

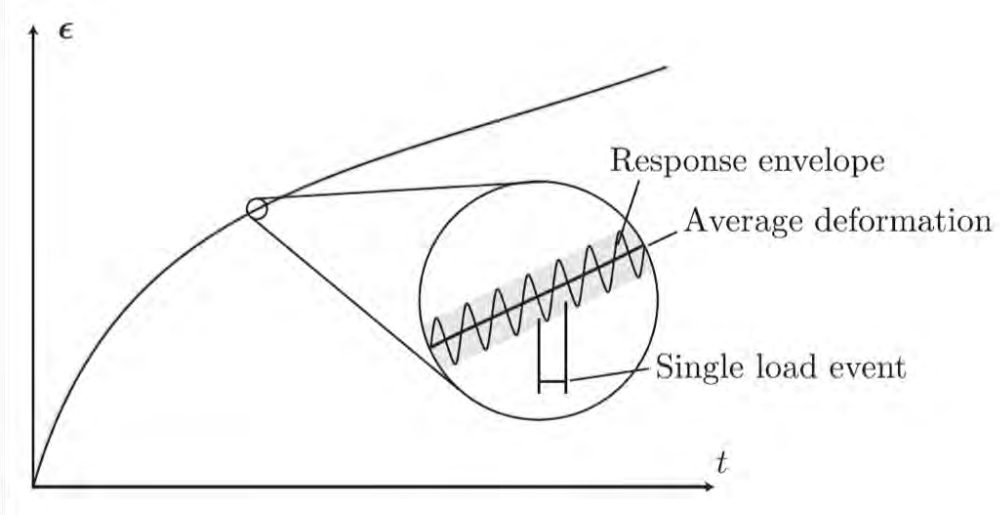


Figure 2.2: *Concept of a explicit strain accumulation function that explicitly relates the time t (or number of cycles) with the accumulated strain ϵ (François et al. 2010)*

The proposed constitutive model to capture strain accumulation in sensitive clays is developed as a *explicit* model, so that it enables to capture the large number of loading cycles associated to railway operation. Furthermore, it is more suitable as hierarchical extension to the Creep-Sclay1s.

2.3.4 Strain accumulation extension for Creep-Sclay1s

A new constitutive model, Creep-Sclay1sc, is developed to explicitly capture the effects from cyclic loading of soft soils, by extending the original Creep-Sclay1s model (Sivasithamparam et al. 2015) with an explicit cumulative viscoplastic multiplier. Full details on the model formulation and calibration are presented in Appendix A.

It is assumed that the total strain tensor ε_{ij} can be decomposed in the elastic ε^e_{ij} and viscoplastic ε^{vp}_{ij} strain components:

$$\varepsilon_{ij} = \varepsilon^e_{ij} + \varepsilon^{vp}_{ij} \tag{2.3}$$

The viscoplastic strain ε^{vp}_{ij} corresponds to the irrecoverable deformation that occurs in the material, and consists of two components:

$$\varepsilon^{vp}_{ij} = \varepsilon^c_{ij} + \varepsilon^{cyc}_{ij} \tag{2.4}$$

ε^c_{ij} which corresponds to the viscoplastic creep strain, and ε^{cyc}_{ij} that represents the additional viscoplastic strain that develops during cyclic loading.

The cyclic cumulative deformation is accounted for by extending the idea of a viscoplastic multiplier, for a non-classic viscoplastic model, having no purely elastic region. The viscoplastic creep strain in the original Creep-Sclay1s model is defined as:

$$\varepsilon^c_{ij} = \dot{\Lambda}\frac{\partial p'_{eq}}{\partial \sigma'_{ij}} \tag{2.5}$$

where p'_{eq} is the equivalent effective mean hydrostatic stress, $\dot{\Lambda}$ the viscoplastic creep multiplier, and σ'_{ij} the effective stress tensor.

The cyclic cumulative strain is incorporated by adding an additional viscoplastic multiplier $\dot{\Omega}$. Equation 2.4 is hence rewritten as:

$$\dot{\varepsilon}_{ij}^{vp} = \left[\dot{\Omega} + \dot{\Lambda}\right] \frac{\partial p'_{eq}}{\partial \sigma'_{ij}} \tag{2.6}$$

This implies that the viscoplastic strain resulting from the cyclic loading follows the same direction as the viscoplastic creep strain, because the associate flow rule is maintained. The cumulative viscoplastic multiplier $\dot{\Omega}$ was derived using a Bailey-Norton power law, commonly used to characterise viscoplasticity:

$$\dot{\Omega} = \frac{\zeta}{t_{ref|0.1\%}} \left(\frac{T}{T_0}\right)^{\Xi} \left(\frac{\bar{\sigma}_d^{cyc}}{\frac{I_1}{3} M(\theta) - (3J_2)^{1/2}}\right)^{\iota} \tag{2.7}$$

where ζ, Ξ, ι and $t_{ref|0.1\%}$ are model parameters, T is the loading period, T_0 the reference period, $\bar{\sigma}_d^{cyc}$ the amplitude of the cyclic deviatoric stress, $M(\theta)$ the stress ratio at critical state, which is a function of Lode angle θ, where I_1 and J_2 are, respectively, the first invariant of the stress tensor and the second invariant of the deviatoric stress tensor. The model parameter ζ can be interpreted as the gradient of the cyclic strain – time plot measured at a reference time $t_{ref|0.1\%}$, at which the deviatoric strain reaches a value of 0.1%. The parameter Ξ expresses the relation between the cyclic tests performed at a loading period T and the cyclic tests performed at a reference period T_0. The inclusion of the period dependency is related to the fact that the Creep-Sclay1s formulation is time-invariant. From the experimental data it was clear that a loading period dependency exists, hence the need for a parameter accounting for it in the viscoplastic multiplier. The denominator $\frac{I_1}{3} M(\theta) - (3J_2)^{1/2}$ in Equation 2.7, represents the distance of the current stress state to the critical state surface.

2.4 Sensitivity analyses

2.4.1 Principles

Sensitivity analysis is a formalised design method to quantify which model parameters, so called model factors, are of most importance within the numerical model. Depending on the numerical model used, these model parameters may include those for the constitutive model, but also the loads or other boundary conditions can be varied. Techniques for sensitivity analyses are divided into local and global approaches. The local methods are computationally efficient and simple to use, however, their results may be misleading for non-linear models, as they do not incorporate the interactions in-between model parameters (Saltelli et al. 2008). In global sensitivity approaches, uncertainty in the output of mathematical or numerical model is explored through the space of all input factors. Therefore, they are capable of capturing the interaction effects among the input factors.

The method of Morris is one of the global methods of screening important input factors for a model. The fundamental idea behind the method is presented in Morris (1991). Morris method follows the elementary effect (EE) calculation. In fact, the measures of the mean and standard deviation of the elementary effects specifies importance of a factor. The Sobol

method is another global sensitivity measure which was introduced by (Sobol 2001). Sobol method quantifies how the variance of the output depends on the uncertain model parameters. Therefore, it is classified as a variance-based method. Sobol sensitivity measures are presented in Table 2.1 (Saltelli et al. 2008; Herman and Usher 2017). The difference between first and total order indices indicates the interaction effects of the parameter with the others.

Table 2.1: Sobol sensitivity indices

First-order index	S_1	The contribution to the output variance by a single model input alone.
Second-order index	S_2	The contribution to the output variance caused by the interaction of two model inputs.
Total-order index	S_T	The contribution to the output variance caused by a model input, including both its first-order effects and all higher-order interactions.

A major advantage of both methods is that they capture the interaction effects between the parameters as well as the main effects of each factor individually. The Morris method, however, only sorts the parameters by relative importance, whereas the Sobol method accurately quantifies the variance. The drawback of the Sobol method is the high computational cost. As long as the intended number of parameters to be varied is low it does not have high computational cost. If the number of input factor increases within the model the Morris method would be more efficient at the expense of absolute accuracy (Saltelli et al. 2008).

2.4.2 Single integration point

In order to benchmark the idea of using general purpose libraries for sensitivity analyses a first implementation used the Sensitivity Analysis Library in Python, the SALib package (Herman and Usher 2017) to study the sensitivity of the model parameters in the Creep-Sclay1s model. The model is implemented in the strain driver that is originally developed by Niemunis (2011). This allows easy configuration of model parameters and boundary conditions (corresponding to different common laboratory tests, or alternatively any arbitrary combination of stress and strain control) via an input file and collecting the data from an output file. To simplify the user interaction the package and file handling are implemented in a Graphical User Interface (GUI) that calls the compiled model + strain driver. The principle is shown in Figure 2.3 and a full description in Gras et al. (2017) which is attached in Appendix B. The single integration point level modelling can be seen as only solving $\{\mathbf{r^{int}}\}$ for a prescribed $\{\mathbf{r^{ext}}\}$ that comes from the strain driver.

Figure 2.4 shows an example output using the Sobol method in conjunction with the Creep-Sclay1s model for the anisotropically consolidated undrained test in compression (left) and the Constant Rate of Strain (CRS) test (right). Two ranges for the parameter variation are shown (range 1: 10% variation on each model parameter and range 2: more realistic measurement uncertainties). What becomes clear is that depending on the loading path, different parameters are affecting the output more than other parameters.

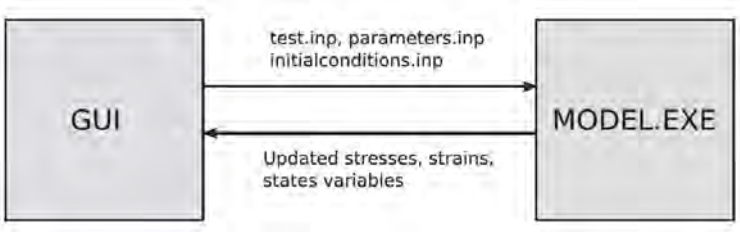


Figure 2.3: *Principle of strain driver with sensitivity analyses; (Gras et al. 2017)*

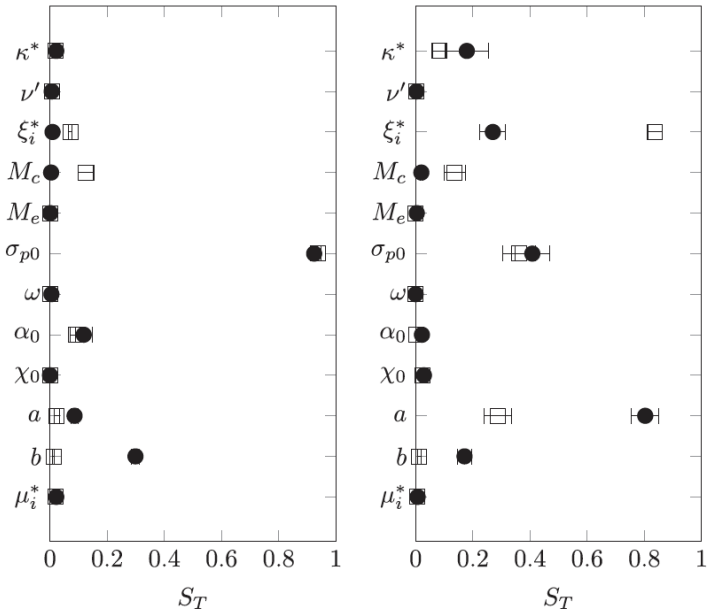


Figure 2.4: *Example result for a sensitivity analyses using the Sobol method for the CAUC triaxial test (left) and the CRS compression test (right); full details in Gras et al. (2017)*

A further feature of the GUI presented in Gras et al. (2017) used here is that it incorporates a multi-objective optimisation tool that is based on the Deap Python library (Fortin et al. 2012). This multi-objective optimisation tool was essential to calibrate the new cyclic accumulation model Creep-Sclay1sc against the data presented in (Wichtmann et al. 2013), see Appendix A.

Given the positive results on using more rigorous sensitivity analyses on single integration point level the method needs to be extended to boundary value level using more elements in a Finite Element code. This allows to model dynamic effects and the coupling with groundwater flow and consolidation. Two features that are not captured at integration point level.

2.4.3 Multi-element level

The lessons learned from the single integration point level analyses are carried over to study the effect of strain accumulation from cyclic loading, as modelled with Creep-Sclay1sc after calibration on the Onsøoy data set presented in (Wichtmann et al. 2013).

The SALib libraries (Herman and Usher 2017) are used in conjunction with a Finite Element code (*Tochnog Professional*) that is easy to script and offers all features required for modelling

dynamic problems in geotechnics. The followed approach at boundary value level is similar to the method for the single integration point, as it uses input and output data parsed via input and output files. First a series of cases with different input parameters are generated, which are subsequently run with the FE code before being analysed for the sensitivity index. The intermediate data of each analysis is stored as this allows to re-evaluate the sensitivity of parameters at different coordinates in the domain without the need to run the analyses again. Furthermore, it allows to study the particular geotechnical response in more detail.

The cases studied at boundary value level will be elaborated in more detail the following Chapter.

3 Strain accumulation below high-speed rail

3.1 Introduction

The newly developed strain accumulation model is used to investigate the effect of loading period T and loading amplitude A on the settlements in a soft sensitive clay below a railway embankment. As such it serves to investigate the relative importance of these two properties on the emerging settlements.

3.2 Embankment on soft soil

3.2.1 Numerical model

An idealised embankment on Onsøy clay has been simulated using *Tochnog Professional*. The model parameters for the constitutive model are summarised in Table 3.1 for the classic model parameters for Creep-Sclay1s and Table 3.2 for the parameters that correspond to the cyclic accumulation part of the model. For practical engineering purposes this approach might be daunting, however, the hierarchical nature of the model allows to calibrate each parameter (**amavasai2017**) in the base model (Creep-Sclay1s) against common laboratory tests. The cyclic model parameters requires more specialised data. A discussion on calibration is elaborated in Appendix A for the cyclic part and Appendix B discusses the approach for multi-objective optimisation of the parameters in the base model (Gras et al. 2017).

The half symmetry plane strain simulation models an embankment of 2 m height, a crest width of 12 m and slope inclination of 1:2. The mesh has 2705 2^{nd} order triangular elements. An Updated Lagrangian formulation has been adopted. In addition to the soft clay that has been modelled using the newly proposed model, the embankment material (height of 2 m) and dry crust (with thickness of 4 m) are modelled using linear elasticity (material properties in Table 3.3). As such the focus is on the the performance of the new model. A fully coupled formulation with the storage equation that models the groundwater flow has been used. The horizontal displacements are constrained at the two side boundaries, whereas the vertical and horizontal displacements are constrained at the bottom boundary. The hydraulic boundaries are closed at the sides and bottom with a free water surface just below the dry crust. A complete overview of the geometry and mesh of the simulated embankment is shown in Figure 3.1. To isolate the performance of the model, this model has no piles incorporated, the impact of deep mixed columns is under investigation in a follow up BIG project.

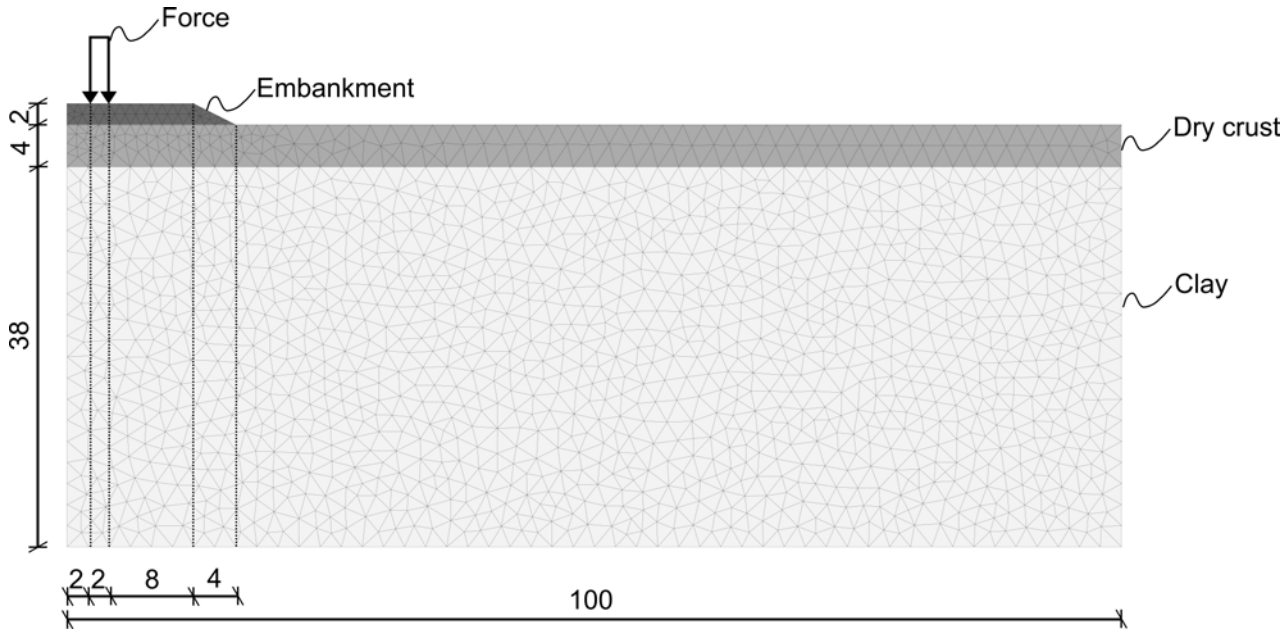


Figure 3.1: *Embankment geometry and finite element mesh.*

Table 3.1: Model parameters for the natural Onsøy clay.

Parameter	Definition	unit	value
λ_i^*	Modified intrinsic compression index	[-]	0.076
κ^*	Modified swelling index	[-]	0.011
ν	Poisson's ratio	[-]	0.15
M_c	Stress ratio at critical state in triaxial compression	[-]	1.23
M_e	Stress ratio at critical state in triaxial extension	[-]	0.80
ω	Rate of rotation	[-]	200
ω_d	Rate of rotation due to deviator strain rate	[-]	0.56
a	Rate of destructuration	[-]	10
b	Rate of destructuration due to deviator strain rate	[-]	0.30
OCR	Over-consolidation ratio	[-]	1.5
e_0	Initial void ratio	[-]	1.80
α_0	Initial anisotropy	[-]	0.47
χ_0	Initial amount of bonding	[-]	10
μ_i^*	Modified intrinsic creep index	[-]	0.005
τ	Reference time	[d]	1

Table 3.2: Cyclic parameters for Creep-SClay1S.

Parameter	Definition	units	value
ζ	Axial strain accumulation factor in undrained cyclic triaxial test	[d]	1.37×10^{-3}
ι	Effectiveness of cyclic deviator stress	[-]	1.83×10^{-4}
Ξ	Loading period dependency	[-]	0.507
Γ_{alpha}	Scaling factor to set cyclic reference time	[-]	2.91×10^{-5}
Γ_{beta}	Scaling factor to set cyclic reference time	[-]	5.92

Table 3.3: Elastic parameters for the embankment and the dry crust.

Material	Parameter	units	value
Embankment	Young's modulus	[kPa]	25×10^3
	Poisson's ratio	[-]	0.3
Dry crust	Young's modulus	[kPa]	7×10^3
	Poisson's ratio	[-]	0.3

In the reference calculation the cyclic loading was simulated by applying a sinusoidal distributed load (with a prescribed frequency of 1 Hz or $1/T$) slightly out of centre on top of the embankment, with a 2 m width and with an amplitude A of 100 kN/m. The load was applied first as one cycle, to capture the amplitude of the cyclic deviatoric stress throughout the domain, which was followed by the application of the cyclic accumulation.

3.2.2 Results reference calculations

Figure 3.2 shows the evolution of the vertical displacement as function of the number of cycles for the point located on the centre line at interface between the embankment and the dry crust. The results of the basic Creep-Sclay1s model without cyclic degradation is also plotted for comparison. Two additional simulations are shown to study the effect of doubling the frequency or the loading amplitude: **scenario 1**, with frequency 2 Hz and a load amplitude of 100 kN/m, and **scenario 2** with a frequency of 1 Hz and a load amplitude of 200 kN/m. The results suggest that the cyclic loading has a significant effect on the predicted vertical displacement. For up to 1000 loading cycles the response predicted by the basic creep model and the new cyclic model is similar. However, for the model parameters selected, after 1000 cycles the effect of the cyclic degradation becomes dominant. It should be noted that the absolute magnitude for the vertical displacements is very large, this is due to the soft clays modelled that typically requires a deep foundation.

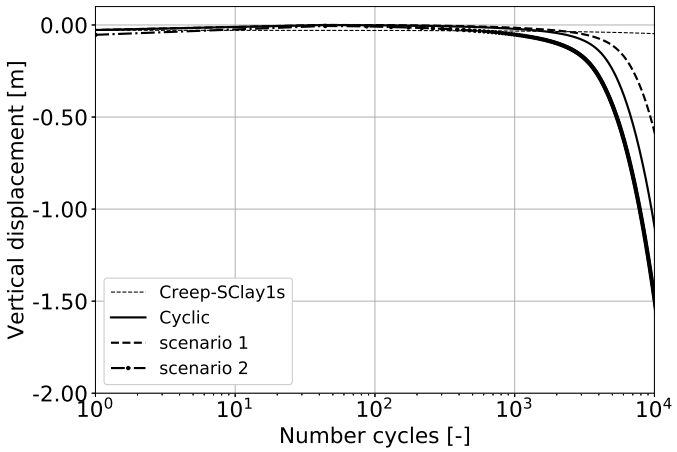


Figure 3.2: *Vertical displacement of the point located along the axis of symmetry at the interface between the embankment and the soil.*

3.3 Sensitivity analyses

3.3.1 Scenarios

A more rigorous sensitivity study is performed in order to further study the sensitivity of the solution for a range of loading amplitudes A and loading periods T (1/frequency). These are the, so called, rank factors that will be studied for their influence upon the output. The range of the two parameters are shown in Table 3.4. These properties are converted so that the maximum amplitude roughly corresponds quadruple the axle load of a X2000 train (at 60 kN for passenger carriages), whilst the period corresponds to train velocities that are centred around a period of 0.32 s (3.5e-6 day) that corresponds to 200 km/h for a 17 m distance between two bogeys. It is noted that the extreme values for the period are more geared to test the model implementation and not necessarily reflect physical realistic train velocities.

Table 3.4: Domain of factors

Factor	Unit	Description	Min	Max
T	[days]	Period	0.35e-6	35e-6
A	[kN]	Amplitude	10	250

The sensitivity of a parameter for (1) the vertical displacements at the centre line and (2) the horizontal displacements at the toe are quantified. In this sensitivity investigation a total number of 600 realisations, i.e. finite elements (FE) runs, were run to perform the analysis.

3.3.2 Results

Firstly, the impact of the loading period T and loading amplitude A on the vertical displacements at the centre line is plotted in Fig. 3.3. The Figure plots the first order index S_1 and the total order index S_T for T and A on the vertical displacements directly below the embankment at the centre line. It becomes apparent that the loading period has the largest impact on the accumulated settlements. This follows the interpretation of the laboratory data, where the period influences the results more directly than the loading amplitude.

The similarity in results between the S_1 and S_T results indicate that there is no interaction between the two properties. Furthermore, the size of the error bar suggests that the number of realisations is sufficient to obtain statistically significant results. More realisations, however, will reduce the length of this error bar. The results are somewhat biased by the modelling approach where to arrive at an equal number of loading cycles the total duration of the analyses is scaled. It simply takes longer to complete 100 000 cycles with a large period. The results, most probably, will be affected in case the comparison was made for an equal calendar time, e.g. 5 y of operation. Though in the latter it is far from trivial to select a representative number of loading cycles.

The results in Fig. 3.4 are obtained when the sensitivity analyses is analysed for the horizontal displacements at the toe of the embankment. Clearly, the main effect is the loading amplitude. This is can be explained by the deviatoric stress distribution in the system which is used for the accumulation stage. The impact of the train load on the deviatoric stress increment at that point is lower than for a point directly below the centre of the embankment.

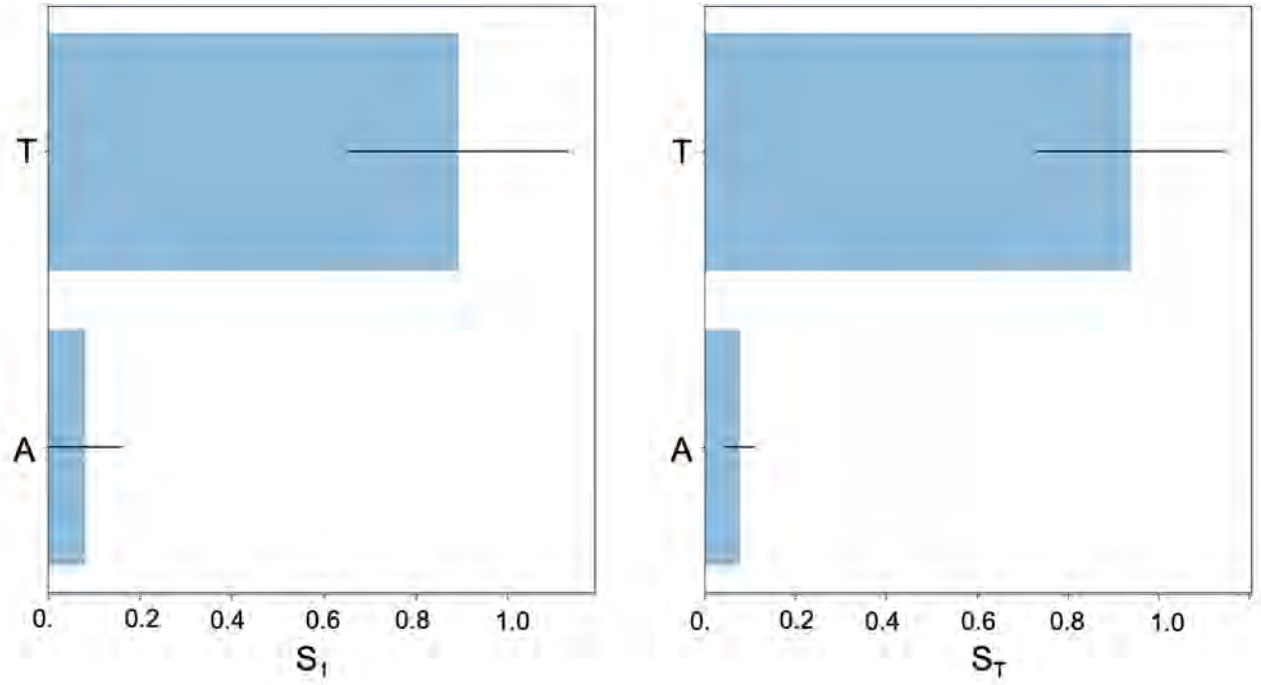


Figure 3.3: *First order S_1 and total order S_T sensitivity index for T and A evaluated from the vertical displacements at the centre line.*

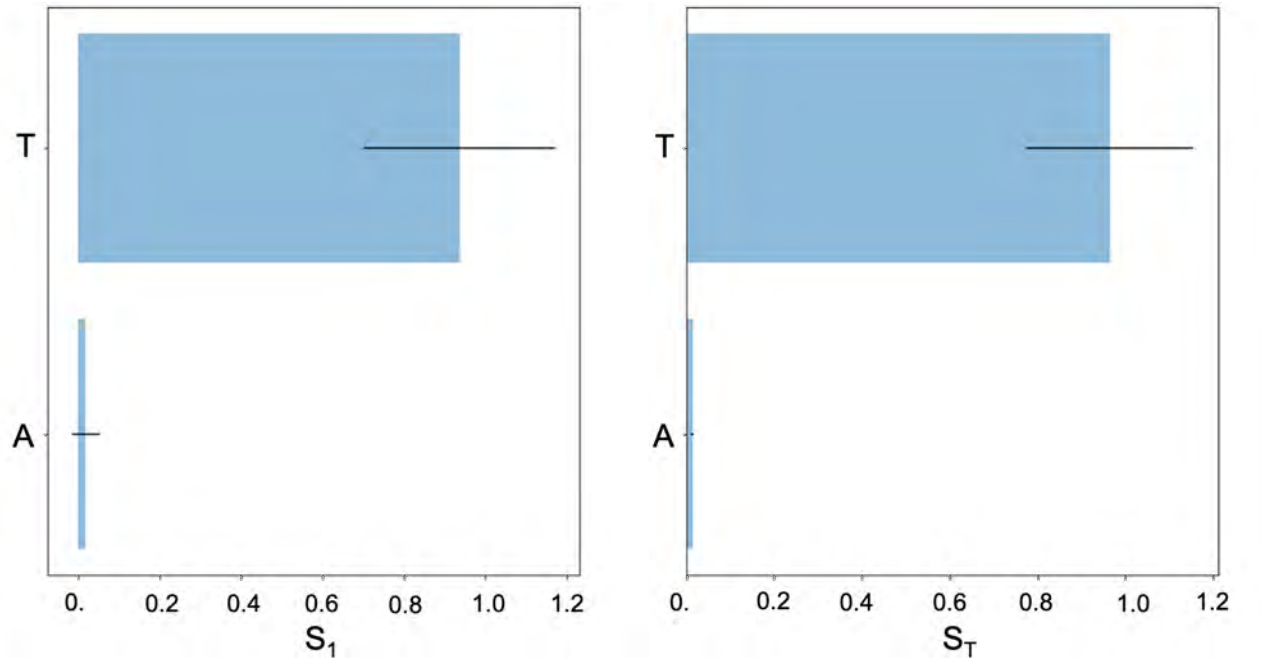


Figure 3.4: *First order S_1 and total order S_t sensitivity index for T and A evaluated from the horizontal displacements at the toe of the embankment.*

Fig. 3.5 plots the total vertical displacements below the centre of the embankment against the number of load cycles. Each line represents one realisation and the mean of all results is plotted in black. A closer investigation of the outliers indicate that the largest vertical displacements are for realisation #271 with a period $T = 3.39\text{e-}5$ days and amplitude $A = 243$ kN, whereas realisation #139 with $T = 3.39\text{e-}7$ days and amplitude $A = 190$ kN led to the smallest accumulated displacements. As long as the amplitude does not lead to large stress levels beyond the pre-consolidation pressure the accumulated cyclic displacements are small and shorter periods further reduce the observed magnitude of vertical displacements. It should be noted that the majority of realisations fall below 0.5 m of total settlements. Although still large, these magnitudes are somewhat more realistic than of the reference case.

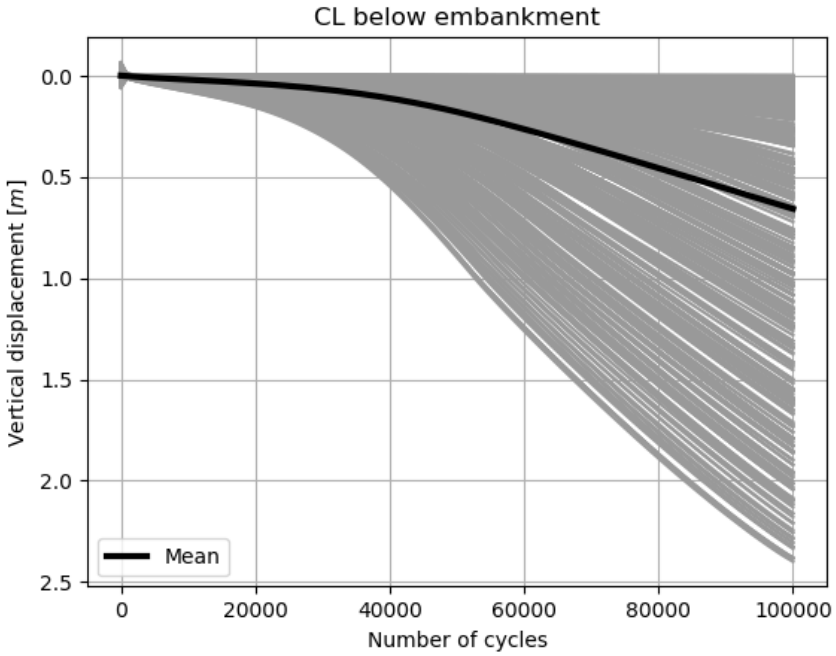


Figure 3.5: *Results of 600 realisations for the calculated vertical displacements of the point located along the axis of symmetry at the interface between the embankment and the soil.*

4 Conclusions & Recommendations

4.1 Conclusions

The report proposes a new constitutive model developed to implicitly capture the effects from cyclic loading of soft soils, by extending the original Creep-Sclay1S model with an explicit cumulative viscoplastic multiplier. The model accounts for the effect of the cyclic loading magnitude, as well as the loading period. All this leads to a computational efficient and numerical stable solution for simulation of a large number of load cycles without encountering numerical issues.

Comparison of model simulations and experimental data on undrained cyclic triaxial tests on block samples of natural Onsøy clay, a high plasticity sensitive clay from Norway that is comparable to the clay in the Gothenburg region, demonstrate that the model is able to predict accurately the rate of strain accumulation, as well as the onset of failure for isotropically and anisotropically consolidated triaxial tests sheared in compression. More cyclic data with varying loading rates in compression and extension are required before the model and parameter determination can be refined.

The model has been shown to work on both single element level and boundary value level. The effects of the cyclic loading have been illustrated for an imaginary railway embankment built on top of a deposit of Onsøy clay. The analyses have highlighted the effect of cyclic loading on the plastic deformations in the soil below the embankment. It was shown that the cyclic component is more significant than creep, and that there is a relation between loading amplitude and loading frequency and the accumulated deformation in the soil. Further systematic sensitivity analyses using the Sobol method further highlights the importance of the cyclic effects on accelerating the settlements below an embankment. The results from 600 cases where the loading magnitude and loading period were varied showed that the results are most sensitive for the loading period. Furthermore, Sobol analyses did not show an interdependence between the loading amplitude and the loading period.

4.2 Recommendations

This research is only a first step towards a full comprehension and modelling capability of the long-term changes in the dynamic response of railway embankments under cyclic loading. The following research activities need to be considered next:

- Establish an experimental link between cyclic accumulation of strain and the dynamic soil properties (stiffness and damping);
- Implement stiffness degradation in the constitutive model presented herein;
- Extend the numerical model to 2D longitudinal sections with moving loads. A transition zone would be a good starting point;
- Complement the quasi-static cyclic accumulation modelling with time-domain dynamic analyses for a single train passage.

References

Adolfsson, K., B. Andréasson, P.E. Bengtson, A. Bodare, C. Madshus, R. Massarch, G. Wallmark, and P. Zackrisson (1999). *High speed lines on soft ground. Evaluation and analyses of measurements from the West Coast Line*. Tech. rep. Banverket.

Coelho, B., P. Hölscher, J. Priest, W. Powrie, and F. Barends (2011). An assessment of transition zone performance. *Proc. of the Institution of Mechanical Engineers, Part F: Journal of Rail and Rapid Transit* **225**.2, 129–139.

Cook, R.D., D. S. Malkus, M. E. Plesha, and R. J. Witt (1989). *Concepts and Applications of Finite Element Analysis,* 3rd ed. John Willey and Sons, New York.

Fortin, Félix-Antoine, François-Michel De Rainville, Marc-André Gardner, Marc Parizeau, and Christian Gagné (July 2012). DEAP: Evolutionary Algorithms Made Easy. *Journal of Machine Learning Research* **13**, 2171–2175.

François, S., C. Karg, W. Haegeman, and G. Degrande (2010). A numerical model for foundation settlements due to deformation accumulation in granular soils under repeated small amplitude dynamic loading. *International Journal for Numerical and Analytical Methods in Geomechanics* **34**.3, 273–296.

Gras, J-P, Nallathamby Sivasithamparam, Minna Karstunen, and Jelke Dijkstra (2018). Permissible range of model parameters for natural fine-grained materials. *Acta Geotechnica* **13**.2, 387–398.

Gras, J.P., N. Sivasithamparam, M. Karstunen, and J. Dijkstra (2017). Strategy for consistent model parameter calibration for soft soils using multi-objective optimisation. *Computers and Geotechnics* **90**, 164–175. ISSN: 0266-352X. DOI: https://doi.org/10.1016/j.compgeo.2017.06.006.

Herman, J. and W. Usher (Jan. 10, 2017). SALib: An open-source Python library for Sensitivity Analysis. *The Journal of Open Source Software* **2**.9, 97. ISSN: 2475-9066. DOI: 10.21105/joss.00097. URL: http://dx.doi.org/10.21105/joss.00097.

Hughes, T.J.R. (2012). *The finite element method: linear static and dynamic finite element analysis*. Courier Corporation.

Karg, C., S. François, W. Haegeman, and G. Degrande (2010). Elasto-plastic long-term behavior of granular soils: Modelling and experimental validation. *Soil Dynamics and Earthquake Engineering* **30**.8, 635–646. ISSN: 0267-7261. DOI: http://dx.doi.org/10.1016/j.soildyn.2010.02.006.

Karstunen, M. and A. Amavasai (2017). *BEST SOIL: Soft soil modelling and parameter determination*. Tech. rep. Chalmers University of technology.

Karstunen, M., H. Krenn, S. Wheeler, M. Koskinen, and R. Zentar (2005). Effect of Anisotropy and Destructuration on the Behavior of Murro Test Embankment. *International Journal of Geomechanics* **5**.2, 87–97.

Leroueil, S. and P.R. Vaughan (1990). The general and congruent effects of structure in natural soils and weak rocks. *Géotechnique* **40**.3, 467–488.

Li, L.-L., H.-B. Dan, and L.-Z. Wang (2011). Undrained behavior of natural marine clay under cyclic loading. *Ocean Engineering* **38**.16, 1792–1805. ISSN: 0029-8018. DOI: http://dx.doi.org/10.1016/j.oceaneng.2011.09.004.

Li, X., M. Ekh, and J.C.O. Nielsen (2016). Three-dimensional modelling of differential railway track settlement using a cycle domain constitutive model. *International Journal for Numerical and Analytical Methods in Geomechanics* **40**.12, 1758–1770.

Lombeart, G., G. Degrande, J. Kogut, and J. François (2006). The experimental validation of a numerical model for the prediction of railway induced vibrations. *Journal of Sound and Vibration* **297**.3, 512–535.

Madshus, C. and A.M. Kaynia (2000). High-speed railway lines on soft ground: dynamic behaviour at critical train speed. *Journal of Sound and Vibration* **231**.3, 689–701.

Morris, Max D (1991). Factorial Sampling Plans for Preliminary Computational Experiments. **33**.2, 161–174.

Mrŏz, Z., V.A. Norris, and O.C. Zienkiewicz (1978). An anisotropic hardening model for soils and its application to cyclic loading. *International Journal for Numerical and Analytical Methods in Geomechanics* **2**.3, 203–221.

Ni, J., B. Indraratna, X. Geng, J. Carter, and Y. Chen (2014). Model of Soft Soils under Cyclic Loading. *International Journal of Geomechanics* **15**.4, 1–10. DOI: 10.1061/(ASCE)GM.1943-5622.0000411.

Niemunis, A. (2011). *Incremental Driver. Programmer's manual*.

Niemunis, A., T. Wichtmann, and Th. Triantafyllidis (2005). A high-cycle accumulation model for sand. *Computers and Geotechnics* **32**.4, 245–263. ISSN: 0266-352X. DOI: http://dx.doi.org/10.1016/j.compgeo.2005.03.002.

Pasten, C., H. Shin, and J. Santamarina (2014). Long-Term Foundation Response to Repetitive Loading. *Journal of Geotechnical and Geoenvironmental Engineering* **140**.4, 1–11.

Saltelli, Andrea, Marco Ratto, Terry Andres, Francesca Campolongo, Jessica Cariboni, Debora Gatelli, Michaela Saisana, and Stefano Tarantola (Dec. 2008). *Global Sensitivity Analysis: The Primer*. January. Chichester, U.K.: John Wiley & Sons, Ltd, p. 312. ISBN: 978-0-470-05997-5. DOI: 10.1002/9780470725184. URL: http://doi.wiley.com/10.1002/9780470725184.ch6%20http://doi.wiley.com/10.1002/9780470725184.

Schevenels, M., G. Degrande, and G. Lombaert (2004). The influence of the depth of the ground water table on free field road traffic induced vibrations. *International Journal for Numerical and Analytical Methods in Geomechanics* **28**.5, 395–419.

Sivasithamparam, N., M. Karstunen, and P. Bonnier (2015). Modelling creep behaviour of anisotropic soft soils. *Computers and Geotechnics* **69**, 46–57. ISSN: 0266-352X.

Sobol, I. M. (2001). Global sensitivity indices for nonlinear mathematical models and their Monte Carlo estimates. **55**, 271–280.

Suiker, A.S.J. and R. de Borst (2003). A numerical model for the cyclic deterioration of railway tracks. *International Journal for Numerical Methods in Engineering* **57**.4, 441–470. ISSN: 1097-0207. DOI: 10.1002/nme.683.

Wegener, D. (2013). "Numerical investigation of permanent soil displacements due to dynamic loading". PhD thesis. Ph. D. thesis, Technische Universität Dresden.

Wheeler, S. J., A. Näätänen, M. Karstunen, and M. Lojander (2003). An anisotropic elastoplastic model for soft clays. *Canadian Geotechnical Journal* **40**.2, 403–418. DOI: 10.1139/t02-119.

Wichtmann, T., K.H. Andersen, M.A. Sjursen, and T. Berre (2013). Cyclic tests on high-quality undisturbed block samples of soft marine Norwegian clay. *Canadian Geotechnical Journal* **50**.4, 400–412. DOI: 10.1139/cgj-2011-0390.

Zienkiewicz, O.C. and T. Shiomi (1984). Dynamic behaviour of saturated porous media; the generalized Biot formulation and its numerical solution. *International journal for numerical and analytical methods in geomechanics* **8**.1, 71–96.

Zuada Coelho, Bruno and Michael A Hicks (2016). Numerical analysis of railway transition zones in soft soil. *Proceedings of the Institution of Mechanical Engineers, Part F: Journal of Rail and Rapid Transit* **230**.6, 1601–1613.

Appendix A - Draft paper on the new strain accumulation model for soft soils

Title: Viscoplastic cyclic degradation model for soft natural soils.

Dr Bruno Zuada Coelho

bruno.zuadacoelho@deltares.nl

Deltares

Department of geo-engineering

P.O. Box 177

2600 MH Delft

The Netherlands

Dr Jelke Dijkstra [1]

jelke.dijkstra@chalmers.se

Chalmers University of Technology

Division of Geo-engineering

SE-41296 Gothenburg

Sweden

phone: +46(0)31-7722120

Prof. Minna Karstunen

minna.karstunen@chalmers.se

Chalmers University of Technology

Division of Geo-engineering

SE-41296 Gothenburg

Sweden

phone: +46(0)31-7722144

Word count: 3910

[1] corresponding author

Abstract : needs to be rewritten. to short

This paper presents a new viscoplastic cyclic degradation model, which is an hierarchical extension of the Creep-SClay1S model, to account for the additional permanent deformations resulting from undrained cyclic loading of natural soft clays. The cyclic cumulative strains are incorporated by means of an additional viscoplastic multiplier. This cyclic viscoplastic multiplier adds four additional model parameters that can be derived from undrained cyclic triaxial tests. The model is calibrated using experimental data from undrained cyclic triaxial tests performed on high quality block samples of natural Onsøy clay, at different average shear stresses, shear stress amplitudes and loading periods. The accuracy of the proposed model is demonstrated by comparing the element level simulations with the experimental data. Best results are obtained for triaxial loading paths in compression on isotropically and anisotropically consolidated samples. The proposed model is further applied to a boundary value problem, where an embankment submitted to cyclic loading is simulated. The use of the new model enables the simulation of the response of cyclic loaded foundations on soft soils where the serviceability limit state over a long period of time is governing the design.

Keywords: Cyclic deformation, Rate dependence; Constitutive modelling; Soft Clay

1 Introduction

Cyclic loading is of importance when a significant variation of the load in time is expected, such as is the case when considering offshore foundations, wind turbines, railway tracks, pipelines and natural slopes [1, 20, 3]. These loads are considered quasi-static, as in most cases the loading period is sufficiently long to disregard the inertial effects in the soil. However, effect of time cannot be disregard due to the non-linear nature of soil behaviour.

The current state of the art for static analysis, such as the bearing capacity of foundations, includes complex non-linear models that in addition to the stability are able to predict, quite accurately, the deformations. However, this accuracy is not yet obtained for problem involving cyclic loading. When complex constitutive models, specifically designed to truthfully capture each loading cycle [16, 5], are used to solve cyclic problems with a large number of loading cycles, $O(10^5)$, issues related to the computational cost and numerical convergence arise. In order to overcome these difficulties, several authors have developed cumulative degradation models to account for the effects of cyclic plastic strains of a large number of loading cycles [11, 17, 18, 19, 23].

However, with exception of the work of [17], all existing models were developed for granular materials. Therefore, there is a lack of models suitable for simulating soft soils. The main limitation of the model presented by [17] for the simulation of cyclic loading on natural soft soils, is that it ignores fundamental soft soil behaviour features, such as rate-dependency, anisotropy and degradation of bonding [13, 25, 12].

In order to overcome the limitations found in the literature, a new constitutive model, Creep-Sclay1Sc, is developed to implicitly capture the effects from cyclic loading of soft soils, by extending the original Creep-Sclay1S model [22] with an explicit cumulative viscoplastic multiplier. The aim of this model it to capture the change in creep rates due to long-term cyclic loading with a reasonable accuracy, and not the development of a fully-fledged model that captures all intricate details under arbitrary loading histories as function of time.

The Creep-Sclay1S modes was chosen as a starting point of this research. It consists

of a viscoplastic rate-dependent model, containing a modified Cam-Clay type of normal compression surface, with rotational and destructuration hardening laws, and where the viscoplastic multiplier is used to model the rate dependency of soft soils (creep).

The first part of this paper presents the description of the Creep-SCLAY1Sc model and discusses the determination of the input parameters for the standard Creep-Sclay1S as well as its extension into cyclic loading. The second part of the paper shows two applications of the model, within the framework of finite element analysis. The first application discusses the performance of the model by comparing the results with experimental undrained cyclic triaxial tests performed on Onsøy clay [26]. The latter application illustrates the robustness of the model by modelling an embankment on soft soil, subjected to cyclic periodic loading, and discusses the effects that loading frequency and amplitude have on the embankment response.

2 Cyclic accumulation model

2.1 Base model: Creep-Sclay1S

The cyclic accumulation model extends the viscoplastic Creep-SClay1S model as presented in [22]. This model accounts for fundamental features of natural soft soil behaviour, such as anisotropy, bonding and rate-dependence [15]. The Creep-Sclay1S model is illustrated in Figure 1 in the p'-q plane. It consists of two reference surfaces: Normal Consolidation Surface (NCS), Current Stress Surface (CSS) and Intrinsic Compression Surface (ICS). The NCS is analogous to the bounding surface and delimits small and large creep strain rates, being defined by the isotropic pre-consolidation pressure p'_m. CSS represents the current effective mean stress state, and it is defined by the mean hydrostatic effective stress p'_{eq}.

One of the main characteristics of the Creep-Sclay1S model is that there is no purely elastic deformation, which means that creep deformation occurs at all stress states. The model predicts an unique critical state, regardless of the strain rate and stress path,

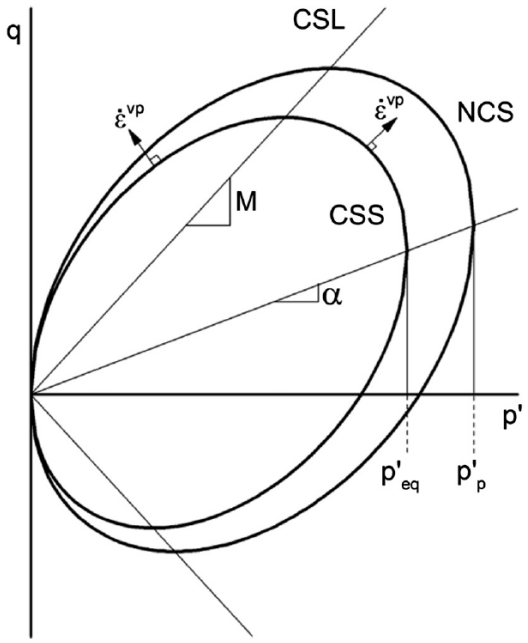


Figure 1: Schematisation of the CreepSClay1S model.

as the NCS rotates as function of plastic shear strains. Results performed with CreepSClay1S model show that the creep behaviour of natural soft soils is correctly captured by the model [22, 2]. However, the model also has limitations, i.e. it is only applicable to normally and slightly overconsolidated clays. Therefore the newly proposed accumulation model inherits these limitations.

Following the classical elasto-plasticity theory, the total strain tensor ε_{ij} can be decomposed in the elastic ε_{ij}^{e} and viscoplastic ε_{ij}^{vp} strain components:

$$\varepsilon_{ij} = \varepsilon_{ij}^{e} + \varepsilon_{ij}^{vp} \tag{1}$$

The viscoplastic strain ε_{ij}^{vp} corresponds to the irrecoverable deformation that occurs in the material, and consists of two components:

$$\varepsilon_{ij}^{vp} = \varepsilon_{ij}^{c} + \varepsilon_{ij}^{cyc} \tag{2}$$

ε_{ij}^{c} which corresponds to the viscoplastic creep strain, and ε_{ij}^{cyc} that represents the

additional viscoplastic strain that develops during cyclic loading.

The cyclic cumulative deformation is accounted for by extending the concept of a viscoplastic multiplier, as presented in [8]. This viscoplastic multiplier is based on a non-classic viscoplastic model, having no purely elastic region. Similarly to most viscoplastic models the viscoplastic multiplier is not deduced from a consistency condition. The viscoplastic creep strain in the Creep-Sclay1S model is defined as:

$$\varepsilon_{ij}^{c} = \dot{\Lambda} \frac{\partial p'_{eq}}{\partial \sigma'_{ij}} \tag{3}$$

where p'_{eq} is the equivalent mean hydrostatic stress, $\dot{\Lambda}$ the viscoplastic creep multiplier, and σ'_{ij} the effective stress tensor.

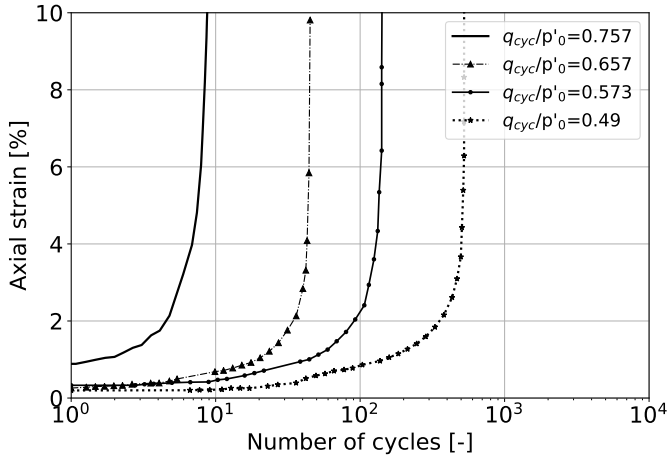
The cyclic cumulative strain is incorporated by adding an additional viscoplastic multiplier $\dot{\Omega}$. Equation 2 is hence rewritten as:

$$\dot{\varepsilon}_{ij}^{vp} = \left[\dot{\Omega} + \dot{\Lambda}\right] \frac{\partial p'_{eq}}{\partial \sigma'_{ij}} \tag{4}$$

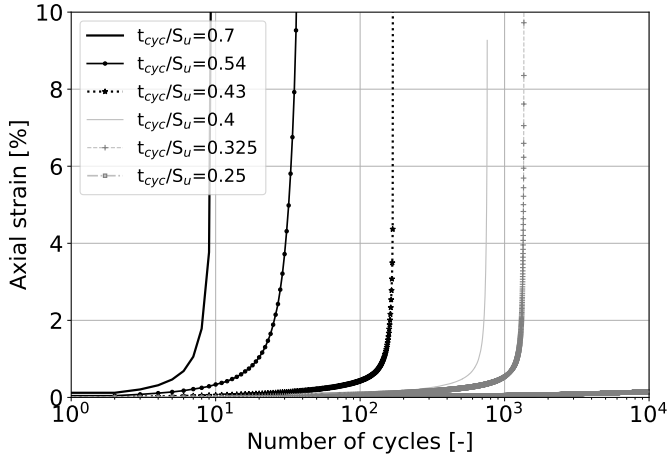
This implies that the viscoplastic strain resulting from the cyclic loading follows the same direction as the viscoplastic creep strain, because the associate flow rule is maintained.

2.2 Cyclic viscoplastic multiplier

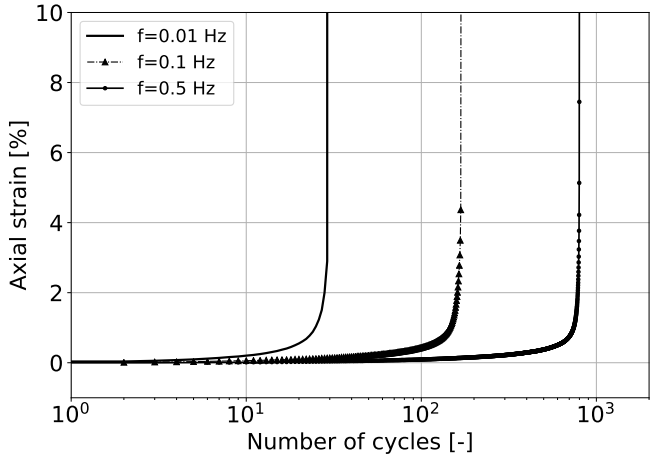
Add plots from them explaining the 3 items



(a)



(b)



(c)

Figure 2: Experimental undrained cyclic triaxial tests: (a) for different cyclic shear strain amplitudes (adapted from [14]), (b) for different cyclic shear strain amplitudes (adapted from [26]) and (c) at different frequencies (adapted from [26]).

The determination of the cylic viscoplastic multiplier has been done, based on experimental evidence from laboratorial cyclic undrained triaxial tests performed by [14] and [26].

Figure 2 summarises the cyclic tests results presented by the authors. From the cyclic experimental triaxial testing, the following observations can be made:

- There is a semi-logarithmic relation between the axial strain and the number of cycles (or time), until the onset of failure;
- The number of cycles required to reach failure reduces with increasing cyclic shear stress amplitude;
- The number of cycles to failure increases with increasing loading frequency.

Based on these observations, the cumulative viscoplastic multiplier $\dot{\Omega}$ was derived using a Bailey-Norton power law, commonly used to characterise viscoplasticity:

$$\dot{\Omega} = \frac{\zeta}{t_{ref|0.1\%}} \left(\frac{T}{T_0} \right)^{\Xi} \left(\frac{\bar{\sigma}_d^{cyc}}{\frac{I_1}{3} M(\theta) - (3J_2)^{1/2}} \right)^{\iota} \tag{5}$$

where ζ, Ξ, ι and $t_{ref|0.1\%}$ are model parameters, T is the loading period, T_0 the reference period, $\bar{\sigma}_d^{cyc}$ the amplitude of the cyclic deviatoric stress, $M(\theta)$ the stress ratio at critical state, which is a function of Lode angle θ, where I_1 and J_2 are, respectively, the first invariant of the stress tensor and the second invariant of the deviatoric stress tensor. The model parameter ζ can be interpreted as the gradient of the cyclic strain measured at a reference time $t_{ref|0.1\%}$, at which the deviatoric strain reaches a value of 0.1%. The parameter Ξ expresses the relation between the cyclic tests performed at a loading period T and the cyclic tests performed at a reference period T_0. The inclusion of the period dependency is related to the fact that the Creep-SClay1S formulation is time-invariant. From the experimental data it was clear that a loading period dependency exists, hence the need for a parameter accounting for it in the viscoplastic multiplier. The denominator $\frac{I_1}{3} M(\theta) - (3J_2)^{1/2}$ in Equation 5, represents to the distance of the current stress state to the critical state surface.

3 Monotonic loading

3.1 Parameter derivation for natural Onsøy clay

The Creep-SClay1Sc model contains 19 model parameters, of which 15 are shared with Creep-Sclay1S as presented in [22]. The parameters for Creep-SClay1Sc can be grouped into five different categories:

- Isotropic parameters (λ_i^*, κ^*, ν, M_c, M_e, OCR, e_0), similar to the Modified Cam-Clay model [21]. The subscript i refers to an intrinsic value;
- Anisotropic parameters (ω, ω_d, α_0), similar to the S-Clay1 model [25];
- Destructuration parameters (a, b, ξ_0), similar to the S-Clay1S model [12];
- Viscosity parameters (μ_i^*, τ), similar to the Creep-SClay1S model [22];
- Cyclic parameters (ζ, Ξ, ι, $t_{ref|0.1\%}$), as presented in Equation 5.

All necessary parameters for the description of Creep-Sclay1Sc, with the exception of the cyclic parameters, can be derived from standard laboratory element tests, such as the combination of undrained monotonic triaxial tests and oedometer tests. The cyclic model parameters requires the additional execution of undrained cyclic triaxial tests. In the current analysis, results on natural Onsøy clay was used to evaluate the performance of the cyclic model, due to the considerable amount of experimental data on high quality block samples of natural clay with both static and cyclic test programmes [3, 4, 7, 26].

The isotropic, anisotropic and destructuration parameters were determined from monotonic triaxial and oedometer tests performed on the natural Onsøy clay [9]. The viscosity parameters μ^* and τ, were determined from triaxial tests on natural Onsøy clay as documented in [10]. Table 1 presents a summary of the adopted parameters. The derivation of the cyclic parameters will be addressed next.

3.2 Monotonic element tests on natural Onsøy clay

Figure 3 shows the comparison between experimental data and the single element level numerical results for monotonic triaxial tests [26] and constant rate of strain compression tests CRSC [9]. The numerical results are in reasonable accordance with the experimental results. Figure 3a shows that, for the triaxial tests in compression, the peak shear stress and slope of the critical state line are predicted well. Furthermore, the experimental results indicate that the stress path is not completely undrained, given there is a reduction of the mean effective stress p' during the initial loading stage. This might be related to sample disturbance, or due to the sample not been fully saturated. Extension paths were more difficult to predict. In such stress path the anisotropy changes considerably, which can be difficult to capture, as discussed for the SClay1 model [25].

Figure 3b illustrates that for an one-dimensional compression tests both viscoelastic and viscoplastic components of the axial strain, as well as the pre-consolidation pressure, are predicted accurately.

4 Cyclic loading

4.1 Calibration of cyclic parameters

The model parameters (ζ, Ξ, ι and $t_{ref|0.1\%}$), were derived from undrained cyclic triaxial tests [26]. The reference time $t_{ref|0.1\%}$ was found to be related to the ratio of the deviatoric cyclic stress and the deviatoric mean stress (Figure 4). Assuming a power relation between $t_{ref|0.1\%}$ and $\bar{\sigma}_d^{cyc}/(I_1/3)_{t=0}$, Equation 5 is reformulated as:

$$\dot{\Omega} = \frac{\zeta}{\Gamma_\alpha \left(\frac{3\bar{\sigma}_d^{cyc}}{I_{1_{t=0}}}\right)^{-\Gamma_\beta}} \left(\frac{T}{T_0}\right)^{\Xi} \left(\frac{\bar{\sigma}_d^{cyc}}{\frac{I_1}{3} M\left(\theta\right) - \left(3J_2\right)^{1/2}}\right)^{\iota} \tag{6}$$

where Γ_α and Γ_β results from a non-linear least squares fit of the experimental data, as shown in Figure 4. The occurrence of negative values for the reference time are prevented by using a power equation, which is a desirable feature from a computational point of

view.

The model parameter Ξ captures the rate effect of the loading frequency (period) on the cyclic accumulation. Figure 5a shows the strain rate for three cyclic triaxial tests performed under similar initial conditions at different loading periods. The results suggest that a relation between the loading period and the deviatoric strain rate can be established. Figure 5b shows the average normalised strain rate for the three loading periods, together with the numerical results after parameter optimisation. The average normalised strain is defined as average ratio between the strain at the loading period T and at the reference period T_0, until the onset of failure.

Although the experimental and numerical results agree, these results are based on the analysis of only three cyclic tests. Therefore, more tests should be conducted in order to further investigate the effect of the loading period.

The model parameters ζ and ι were obtained by means of mono-objective optimisation of the cyclic triaxial tests [6]. The current analysis only considered the triaxial tests that recorded more than 30 cycles to failure.

Figure 6 summarises the values of the model parameters ζ and ι for all the analysed tests. It was found that the values of ζ, with the exception of three tests, namely 16, 17 & 19, fall within the same range. The parameter ι turns out to be one order of magnitude smaller than parameter ζ, with a similar amount of scatter. This scatter is most probably related to the fact that the Onsøy clay is a natural clay. Substantially more test data would be required to have clear trends in the data that are not affected by the typical sampling/test related scatter.

Table 2 summarises the cyclic parameters for the Creep-SClay1Sc model (Equation 6).

4.2 Cyclic triaxial tests on natural Onsøy clay

The performance of the Creep-SClay1Sc on the modelling of cyclic loading was assessed by comparing the numerical results with experimental undrained cyclic triaxial tests [26], for

a single integration point. Figure 7 presents the comparison between the experimental data and the numerical results for four different cyclic triaxial tests. In general, the numerical and experimental results compare favourably.

Figure 7a illustrates that the new model is able to correctly predict the accumulation of deviatoric strain in a cyclic compression test until the onset of failure. The moment failure occurs, the experimental results show that the strain develops at a higher rate than predicted by the numerical simulation. This is likely related to the fact that the numerical results were obtained on a single integration point, which does not model the development of localised shear bands, and therefore is not able to capture the correct failure mechanism. The expectation is that the predictions will improve in case the same analysis is conducted at boundary value level.

Figure 7b presents a cyclic triaxial test performed with a loading period of 100 s. The deviatoric strain accumulation, as well as the onset of failure again are correctly captured by the Creep-SClay1Sc model. Therefore, the rate effect from the loading period is properly incorporated in the model.

The same applies for the isotropic cyclic triaxial tests (Figure 7c), and it should be noted that for this test no failure was recorded or predicted. The isotropic consolidation paths in the latter tests gradually destroys all bonds in the natural samples, and perhaps this prevents the generation of additional pore water pressures resulting from the collapse of the fabric.

Similarly to the monotonic test results the simulation of the triaxial extension test was not as accurate as the predictions for compression (Figure 7d). Both the strain rate as well as the number of cycles required to the onset of failure are overestimated by the Creep-SClay1Sc model. Since only data from one triaxial test in extension was available, it is not possible to assess whether the difference between the numerical and experimental results are representative. There could have been issues for example due to inhomogeneities within the sample, the necking of the sample or membrane effects, or some other unknown experimental inaccuracies.

5 Boundary value level modelling

5.1 Additional modifications

The main modification required for implementation of the model at boundary value level relates to initialisation of the state variables in each integration point. Furthermore, an appropriate amplitude for the cyclic deviatoric stress $\bar{\sigma}_d^{cyc}$ that drives the magnitude of strain accumulation, needs to be computed depending on the position in the domain. The most convenient manner to address the pre-initialisation is to perform a nill step, i.e. a regular static calculation applying one cycle of the boundary loads, which retrieves the magnitude of the amplitude of cyclic deviatoric stress $\bar{\sigma}_d^{cyc}$ in each integration point. After this nill step, the cyclic accumulation model component (which is a hierarchical formulation) is switched on using a Boolean switch parsed via the Finite Element solver.

5.2 Cyclic triaxial test

An 2D axisymmetric modelling approach was used to model an undrained triaxial test on a sample of 54 mm diameter times 108 mm height at boundary value level. Figure 8 shows the dimensions and mesh of the simulated triaxial test. The domain is meshed with a total of 217 quadrilateral elements using second order shape functions, with 8 nodes in each element. The displacements were constrained along the horizontal direction along the centre axis, and vertically along the bottom edge. The top and outer boundary have a distributed load that is in equilibrium with the anisotropic stress state after consolidation. All flow boundaries are impermeable, and the initial pore pressures are set at 600 kPa. The model parameters for the material are similar to those presented in Tables 1 and 2. Additionally, a groundwater formulation, where the material deformation tensor is coupled to the storage equation has been used with a water density of 1000 kg/$m3$, a bulk stiffness for the water of 10^6 kPa and a hydraulic conductivity of 1.e-9 m/s. The remaining (cyclic) loading conditions correspond to test 31, which is already presented in Figure 7a).

The result of the boundary value analysis is plotted in Figure 9 with the experimental data and the single point results as comparison. The initialisation of the cyclic component of the load is visible, as well as the correctness of the modelling strategy. The small differences between the single point and multi element simulations are expected, given absence of localisation at small strain magnitudes that is further promoted by the regular mesh and axisymmetric boundary conditions used.

After the successful verification of the model implementation at boundary value level using a fully coupled formulation the model is ready to be used in a more demanding boundary value problem.

5.3 Embankment on soft soil

In order to illustrate the benefits of using the proposed cyclic model for modelling a large number of load cycles at boundary value level an idealised embankment on Onsøy clay has been simulated using Tochnog Professional [24].

The half symmetry plane strain simulation models an embankment of 2 m height, a crest width of 12 m and slope inclination of 1:2. The mesh has 2705 2^{nd} order triangular elements. An Updated Lagrangian formulation has been adopted. In addition to the soft clay that has been modelled using the newly proposed model, the embankment material (height of 2 m) and dry crust (with thickness of 4 m) are modelled using linear elasticity (material properties in Table 3). As such the focus is on the the performance of the new model. Similar to the boundary value simulation at element level, a fully coupled formulation with the storage equation has been used. The horizontal displacements are constrained at the two side boundaries, whereas the vertical and horizontal displacements are constrained at the bottom boundary. The hydraulic boundaries are closed at the sides and bottom with a free water surface just below the dry crust. A complete overview of the geometry and mesh of the simulated embankment is shown in Figure 10.

The cyclic loading was simulated by applying a sinusoidal distributed load (frequency 1 Hz) slightly out of centre on top of the embankment, with a 2 m width and 100 kN/m

amplitude. Similar to the triaxial test, the load was applied first as one cycle, to capture the amplitude of the cyclic deviatoric stress, which was followed by the application of the cyclic accumulation.

Figure 11 shows the development of the displacement and strain fields at different number of loading cycles. Up to 2500 load cycles there is little deformation of the embankment (Figures 11a and 11b). As the number of loading cycles increases, the deformation levels increase as well as the strain levels. The largest displacements occur underneath the embankment, while the largest strain is registered in the soft clay layer. As the number of loading cycles increases, a displacement zone starts developing outwards, forming a shear failure.

Figure 12 shows the evolution of the vertical displacement as function of the number of cycles for the point located at the interface between the embankment and the dry crust. The results of the basic creep model without cyclic degradation is also plotted as comparison. Two additional simulations are shown to study the effect of doubling the frequency or the loading amplitude: scenario 1, with frequency 2 Hz and a load amplitude of 100 kN/m, and scenario 2 with a frequency of 1 Hz and a load amplitude of 200 kN/m. The results suggest that the cyclic loading has a significant effect on the predicted vertical displacement. For up to 1000 loading cycles the response predicted by the basic creep model and the new cyclic model is similar. However, after 1000 cycles the effect of the cumulative straining due to cyclic degradation becomes dominant.

The displacement is predicted to reduce with the increase of the loading frequency, which is in agreement with the experimental findings in literature [14, 26]. The load has a direct relation with the displacement, as an increase in the load leads to an increase in the vertical displacement of the embankment. It should be noted that the predicted displacements in these analyses are very high. This is related to the low strength and stiffness of the Onsøy clay tested (both site conditions and block samples from shallow depth), which is assumed to apply for the complete clay layer, without correcting for the in-situ OCR profile.

6 Conclusions

The present paper proposes a new constitutive model developed to implicitly capture the effects from cyclic loading of soft soils, by extending the original Creep-Sclay1S model with an explicit cumulative viscoplastic multiplier. The strain accumulation due to cyclic loading is accounted for by means of a viscoplastic multiplier, in a similar manner to creep. The model extensions adds four additional model parameters, which can be determined from undrained cyclic triaxial test data. The model accounts for the effect of the cyclic loading magnitude, as well as the loading period. All this leads to a computational efficient and numerical stable solution for simulation of a large number of load cycles without encountering numerical issues.

Comparison of model simulations and experimental data on undrained cyclic triaxial tests on block samples of natural Onsøy clay demonstrate that the model is able to predict accurately the rate of strain accumulation, as well as the onset of failure for isotropically and anisotropically consolidated triaxial tests sheared in compression. For loading paths in extension the model underpredicts both the strain rate and the number of cycles to failure, i.e. the results are non-conservative. It must be realised, however, that only one extension triaxial test was available. A power relation between the loading period and the reference loading period T_{ref} was derived using only three cyclic triaxial tests. More cyclic data with varying loading rates in compression and extension are required before the model and parameter determination can be refined.

The model has been shown to work on both single element level and boundary value level. The effects of the cyclic loading have been illustrated for an imaginary railway embankment built on top of a deposit of Onsøy clay. The analyses have highlighted the effect of cyclic loading on the plastic deformations in the soil below the embankment. It was shown that the cyclic component is more significant than creep, and that there is a relation between loading amplitude and loading frequency and the accumulated deformation in the soil.

The proposed new model will offer new insight into the cyclic response of soft soils.

In addition to its capability to correctly model soft soil under monotonic load, the model offers the possibility to simulate large numbers of load cycles in an efficient and accurate fashion. This enables the simulation of the response of cyclic loaded foundations on soft soils where serviceability limit state over a long period of time is governing the design. The latter includes railway embankments and wind turbine foundations.

7 Acknowledgements

The financial support from Trafikverket in the framework of BIG (Branch samverkan i Grund) is greatly acknowledged. JD is supported by a Marie Curie Fellowship grant EC/FP7-MC-IEF 623613 EMPIRIC.

References

[1] Malek Abdelkrim, Guy Bonnet, and Patrick de Buhan. A computational procedure for predicting the long term residual settlement of a platform induced by repeated traffic loading. *Computers and Geotechnics*, 30(6):463 – 476, 2003.

[2] Amardeep Amavasai, Nallathamby Sivasithamparam, Jelke Dijkstra, and Minna Karstunen. Consistent Class A & C predictions of the Ballina test embankment. *Computers and Geotechnics*, 93:75–86, January 2018.

[3] K.H. Andersen. Bearing capacity under cyclic loading offshore, along the coast, and on land. the 21st Bjerrum lecture presented in Oslo, 23 November 2007. *Canadian Geotechnical Journal*, 46(5):513–535, 2009.

[4] T. Berre. Test fill on soft plastic marine clay at Onsøy, Norway. *Canadian Geotechnical Journal*, 51(1):30–50, 2014.

[5] Yannis F. Dafalias and Majid T. Manzari. Simple Plasticity Sand Model Accounting for Fabric Change Effects. *Journal of Engineering Mechanics*, 130(6):622–634, 2004.

[6] J.-P. Gras, N. Sivasithamparam, M. Karstunen, and J. Dijkstra. Strategy for consistent model parameter calibration for soft soils using multi-objective optimisation. *Computers and Geotechnics*, 90:164–175, 2017.

[7] G. Grimstad, M. Mehli, and H.P. Jostad. Settlement analysis of Onsøy test fill. Technical report, NGI, 2014.

[8] Gustav Grimstad, Samson Abate Degago, Steinar Nordal, and Minna Karstunen. Modeling creep and rate effects in structured anisotropic soft clays. *Acta Geotechnica*, 5(1):69–81, 2010.

[9] H.P. Jostad and T. Berre. Additional tests on block samples in connection with the Onsøy test fill. Technical report, NGI, 2010.

[10] H.P. Jostad and J. Yannie. A procedure for determining long-term creep rates of soft clays by triaxial testing. In J. Dijkstra, M. Karstunen, J.-P. Gras, and M. Karlsson, editors, *Proceedings of the International Conference on Creep and Deformation Characteristics in Geomaterials*, pages 39–42. Chalmers University of Technology, 2015.

[11] C. Karg, S. François, W. Haegeman, and G. Degrande. Elasto-plastic long-term behavior of granular soils: Modelling and experimental validation. *Soil Dynamics and Earthquake Engineering*, 30(8):635–646, 2010.

[12] M. Karstunen, H. Krenn, S. Wheeler, M. Koskinen, and R. Zentar. Effect of anisotropy and destructuration on the behavior of Murro test embankment. *International Journal of Geomechanics*, 5(2):87–97, 2005.

[13] S. Leroueil and P.R. Vaughan. The general and congruent effects of structure in natural soils and weak rocks. *Géotechnique*, 40(3):467–488, 1990.

[14] Ling-Ling Li, Han-Bo Dan, and Li-Zhong Wang. Undrained behavior of natural marine clay under cyclic loading. *Ocean Engineering*, 38(16):1792 – 1805, 2011.

[15] J.K. Mitchell and K. Soga. *Fundamentals of Soil Behavior*. Wiley, 3 edition, 2005.

[16] Z. Mrŏz, V.A. Norris, and O.C. Zienkiewicz. An anisotropic hardening model for soils and its application to cyclic loading. *International Journal for Numerical and Analytical Methods in Geomechanics*, 2(3):203–221, 1978.

[17] J. Ni, B. Indraratna, X. Geng, J. Carter, and Y. Chen. Model of soft soils under cyclic loading. *International Journal of Geomechanics*, 15(4):1–10, 2014.

[18] A. Niemunis, T. Wichtmann, and Th. Triantafyllidis. A high-cycle accumulation model for sand. *Computers and Geotechnics*, 32(4):245 – 263, 2005.

[19] C. Pasten, H. Shin, and J. Santamarina. Long-term foundation response to repetitive

loading. *Journal of Geotechnical and Geoenvironmental Engineering*, 140(4):1–11, 2014.

[20] Claudio Di Prisco and Clara Zambelli. Cyclic and dynamic mechanical behaviour of granular soils: experimental evidence and constitutive modelling. *Revue Franaise de Gnie Civil*, 7(7-8):881–910, 2003.

[21] K.H. Roscoe and J.B. Burland. On the generalized stress-strain behaviour of wet clay. In J. Heyman and F.A. Leckie, editors, *Engineering Plasticity*, pages 553–609. Cambridge University Press, 1968.

[22] Nallathamby Sivasithamparam, Minna Karstunen, and Paul Bonnier. Modelling creep behaviour of anisotropic soft soils. *Computers and Geotechnics*, 69:46 – 57, 2015.

[23] Akke S. J. Suiker and René de Borst. A numerical model for the cyclic deterioration of railway tracks. *International Journal for Numerical Methods in Engineering*, 57(4):441–470, 2003.

[24] Tochnog Professional. http://www.feat.nl, 2017.

[25] Simon J Wheeler, Anu Näätänen, Minna Karstunen, and Matti Lojander. An anisotropic elastoplastic model for soft clays. *Canadian Geotechnical Journal*, 40(2):403–418, 2003.

[26] T. Wichtmann, K.H. Andersen, M.A. Sjursen, and T. Berre. Cyclic tests on high-quality undisturbed block samples of soft marine Norwegian clay. *Canadian Geotechnical Journal*, 50(4):400–412, 2013.

8 Captions

List of Figures

1 Schematisation of the CreepSClay1S model.

2 Experimental undrained cyclic triaxial tests: (a) for different cyclic shear strain amplitudes (adapted from [14]), (b) for different cyclic shear strain amplitudes (adapted from [26]) and (c) at different frequencies (adapted from [26]).

3 Comparison of experimental and numerical results: (a) undrained monotonic triaxial test and (b) Constant rate of strain consolidation test.

4 Relation between the cyclic reference time $t_{ref|0.1\%}$ and the stress ratio $\bar{\sigma}_d^{cyc}/(I_1/3)_{t=0}$.

5 Effect of the period of cyclic loading on the undrained cyclic triaxial test results on natural Onsøi clay: (a) deviatoric strain rate and (b) normalised average strain rate.

6 Cyclic model parameters for the undrained cyclic triaxial tests on natural Onsøy clay: (a) ζ and (b) ι.

7 Comparison of experimental and numerical results for cyclic undrained triaxial test: (a) test 31 (compression - period 10 s), (b) test 21 (compression - period 100 s) (c) test 23 (isotropic - period 10 s) and (d) test 17 (extension - period 10 s).

8 Finite element mesh of the triaxial test as a boundary value problem.

9 Axial strain from the triaxial test simulated as the boundary value problem.

10 Embankment geometry and finite element mesh.

11 Displacement and strain fields for different number of loading cycles: (a) and (b) 1, (c) and (d) 2 500, (e) and (f) 5 000, (g) and (h) 10 000.

12 Vertical displacement of the point located along the axis of symmetry at the interface between the embankment and the soil.

List of Tables

1 Model parameters for the natural Onsøy clay.

2 Cyclic parameters for Creep-SClay1S.

3 Elastic parameters for the embankment and the dry crust.

9 Tables

Table 1: Model parameters for the natural Onsøy clay.

Parameter	Definition	unit	value
λ_i^*	Modified intrinsic compression index	[-]	0.076
κ^*	Modified swelling index	[-]	0.011
ν	Poisson's ratio	[-]	0.15
M_c	Stress ratio at critical state in triaxial compression	[-]	1.23
M_e	Stress ratio at critical state in triaxial extension	[-]	0.80
ω	Rate of rotation	[-]	200
ω_d	Rate of rotation due to deviator strain rate	[-]	0.56
a	Rate of destructuration	[-]	10
b	Rate of destructuration due to deviator strain rate	[-]	0.30
OCR	Over-consolidation ratio	[-]	1.5
e_0	Initial void ratio	[-]	1.80
α_0	Initial anisotropy	[-]	0.47
χ_0	Initial amount of bonding	[-]	10
μ_i^*	Modified intrinsic creep index	[-]	0.005
τ	Reference time	[d]	1

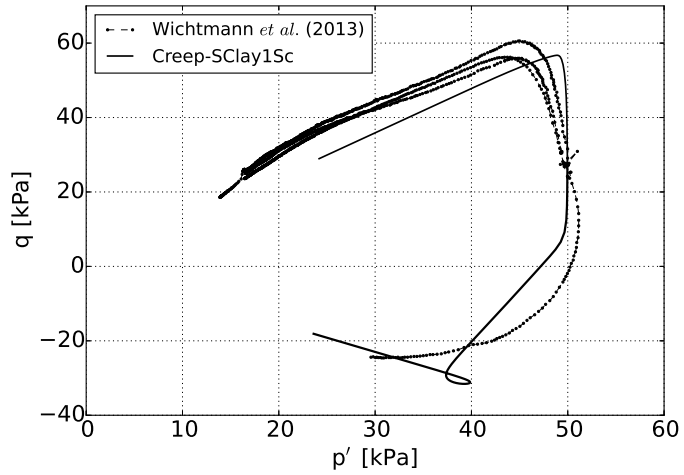
Table 2: Cyclic parameters for Creep-SClay1S.

Parameter	Definition	units	value
ζ	Axial strain accumulation factor in undrained cyclic triaxial test	[d]	1.37×10^{-3}
ι	Effectiveness of cyclic deviator stress	[-]	1.83×10^{-4}
Ξ	Loading period dependency	[-]	0.507
Γ_{alpha}	Scaling factor to set cyclic reference time	[-]	2.91×10^{-5}
Γ_{beta}	Scaling factor to set cyclic reference time	[-]	5.92

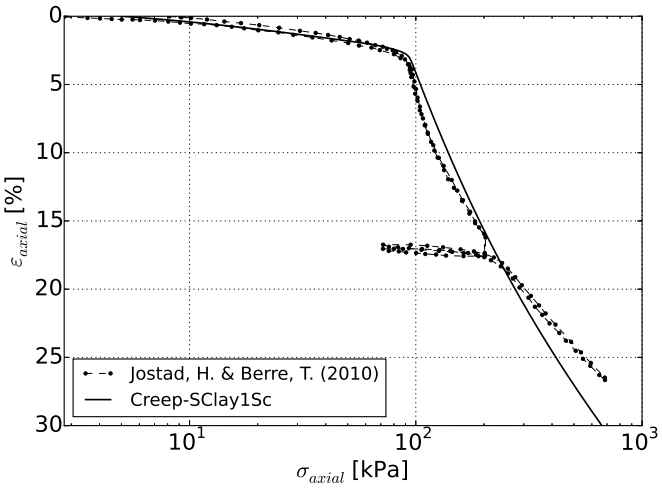
Table 3: Elastic parameters for the embankment and the dry crust.

Material	Parameter	units	value
Embankment	Young's modulus	[kPa]	25×10^3
	Poisson's ratio	[-]	0.3
Dry crust	Young's modulus	[kPa]	7×10^3
	Poisson's ratio	[-]	0.3

10 Figures



(a)



(b)

Figure 3: Comparison of experimental and numerical results: (a) undrained monotonic triaxial test and (b) Constant rate of strain consolidation test.

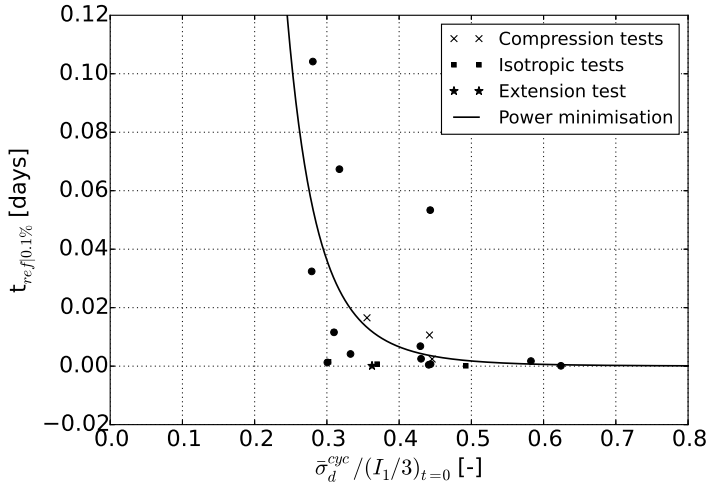
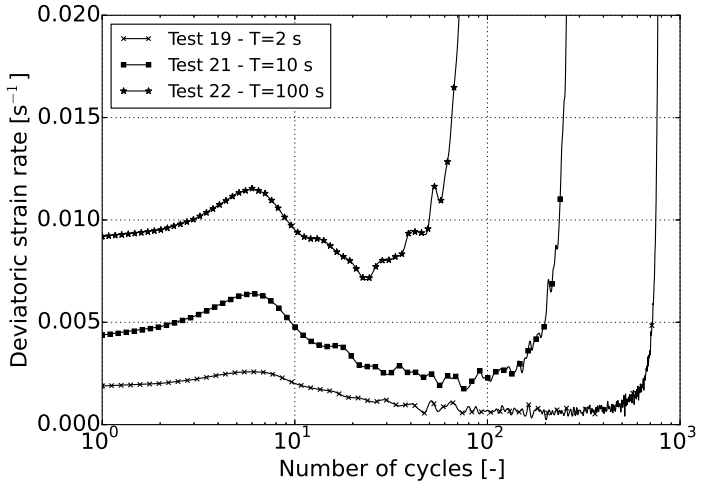
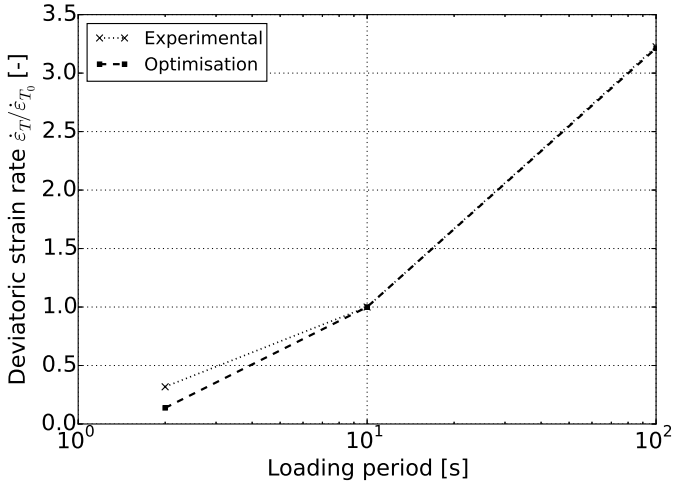


Figure 4: Relation between the cyclic reference time $t_{ref|0.1\%}$ and the stress ratio $\bar{\sigma}_d^{cyc}/(I_1/3)_{t=0}$.

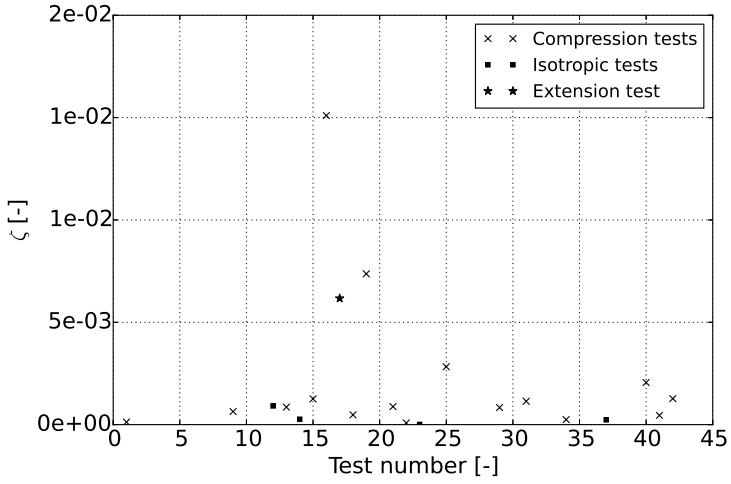


(a)

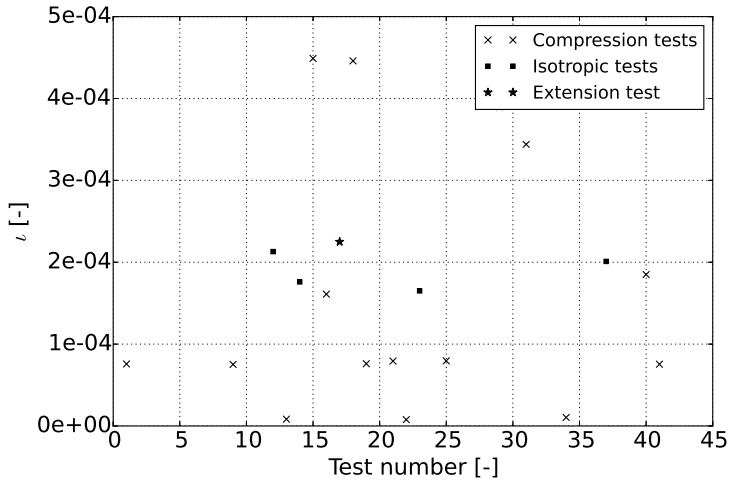


(b)

Figure 5: Effect of the period of cyclic loading on the undrained cyclic triaxial test results on natural Onsøi clay: (a) deviatoric strain rate and (b) normalised average strain rate.

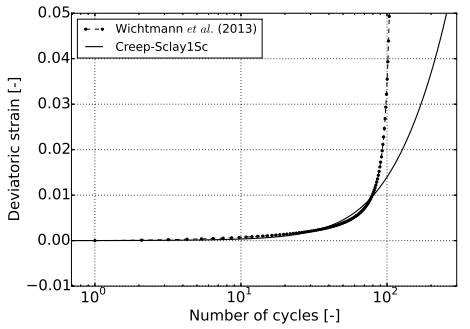


(a)

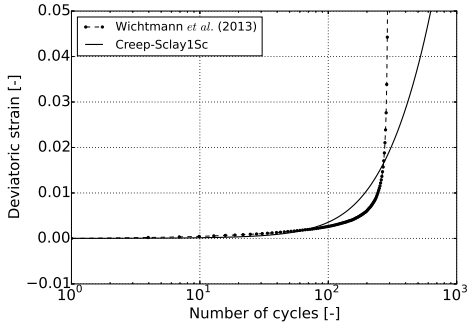


(b)

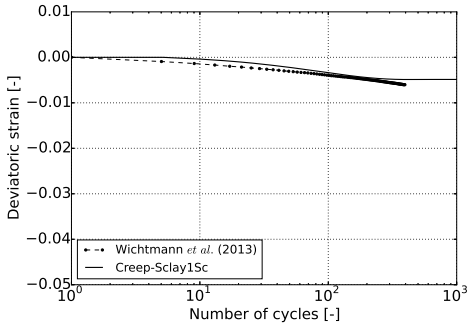
Figure 6: Cyclic model parameters for the undrained cyclic triaxial tests on natural Onsøy clay: (a) ζ and (b) ι.



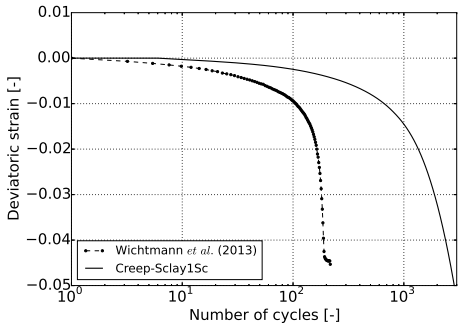
(a)



(b)



(c)



(d)

Figure 7: Comparison of experimental and numerical results for cyclic undrained triaxial test: (a) test 31 (compression - period 10 s), (b) test 21 (compression - period 100 s) (c) test 23 (isotropic - period 10 s) and (d) test 17 (extension - period 10 s).

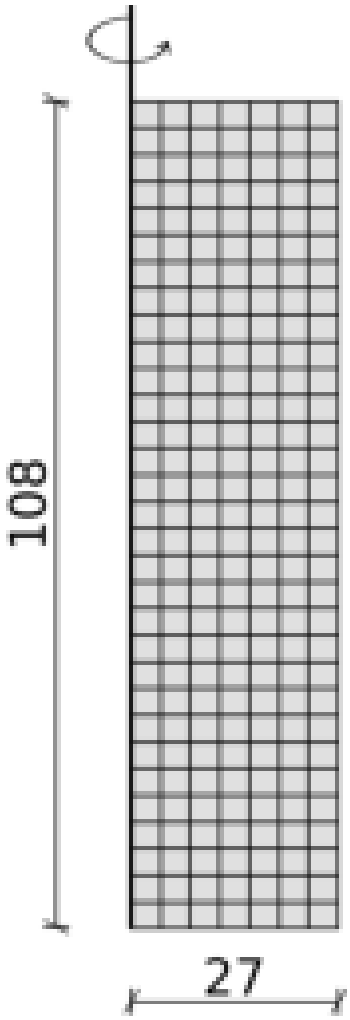


Figure 8: Finite element mesh of the triaxial test as a boundary value problem.

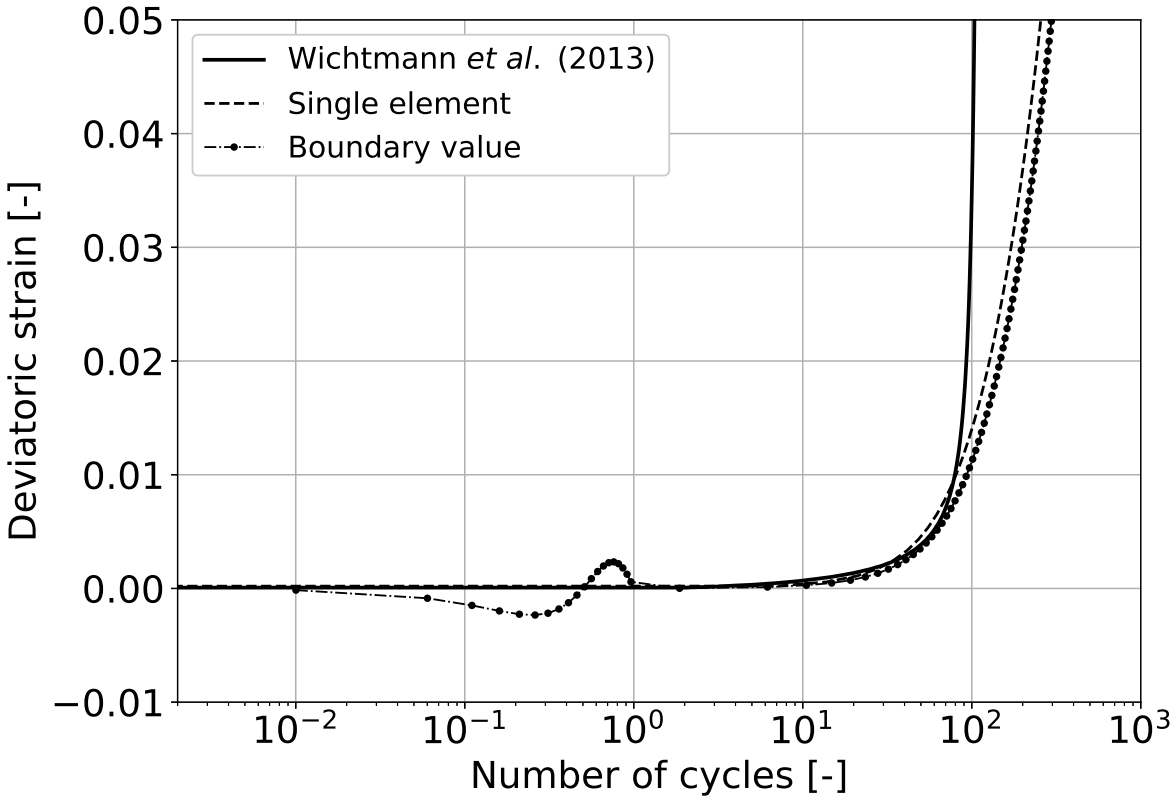


Figure 9: Axial strain from the triaxial test simulated as the boundary value problem.

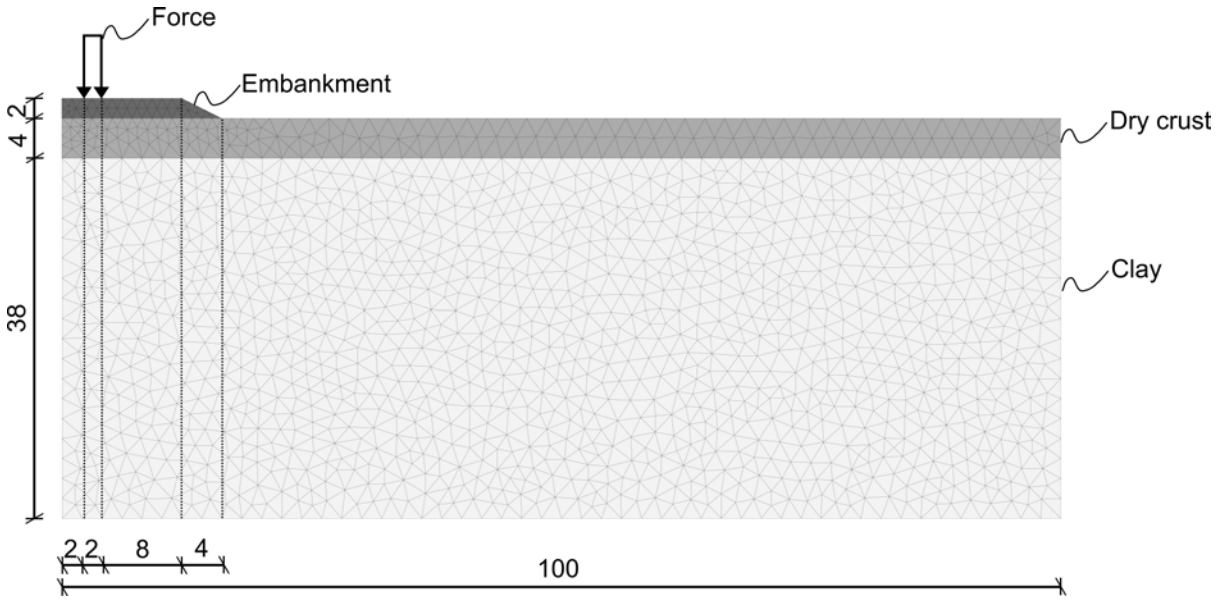


Figure 10: Embankment geometry and finite element mesh.

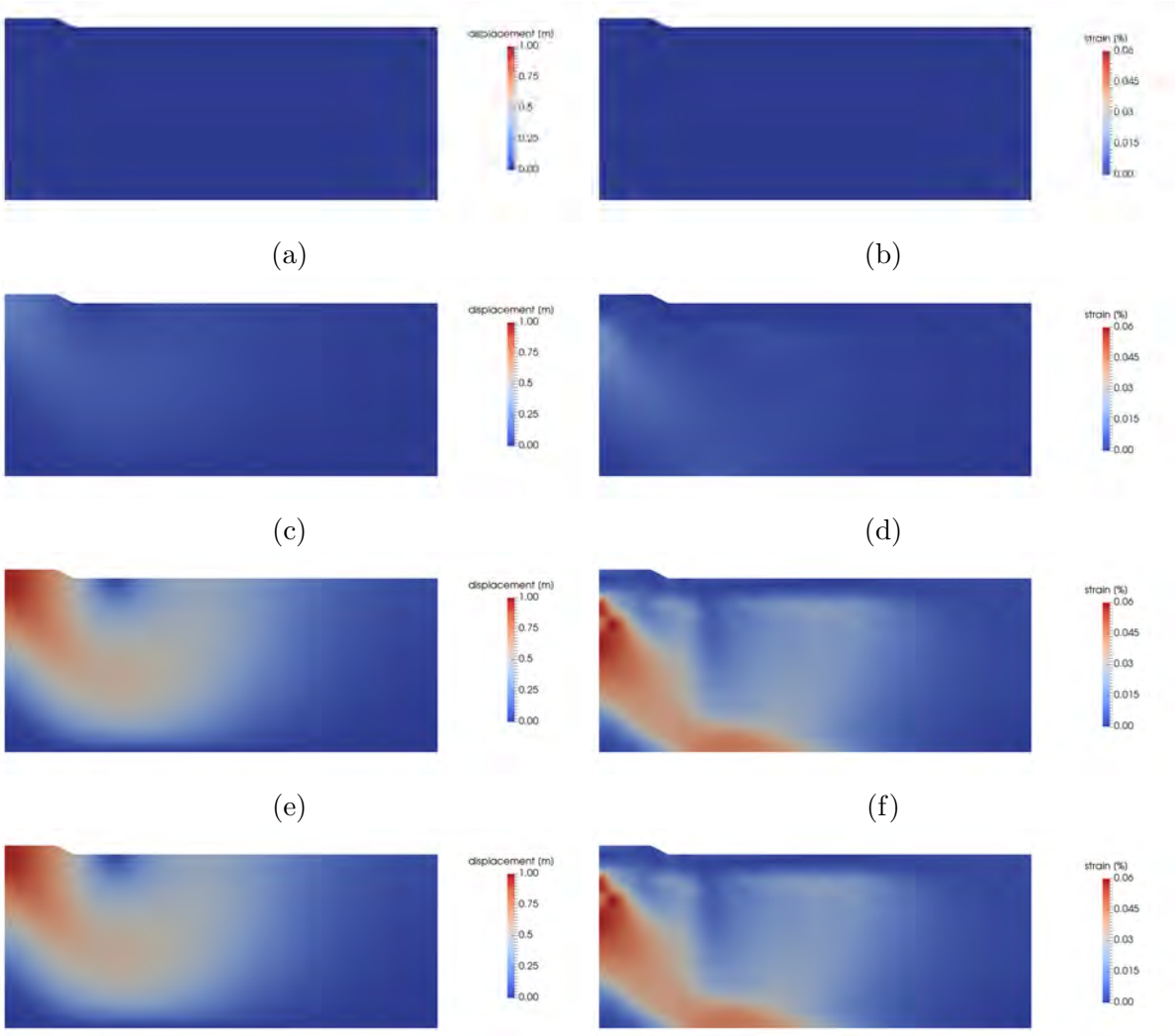


Figure 11: Displacement and strain fields for different number of loading cycles: (a) and (b) 1, (c) and (d) 2 500, (e) and (f) 5 000, (g) and (h) 10 000.

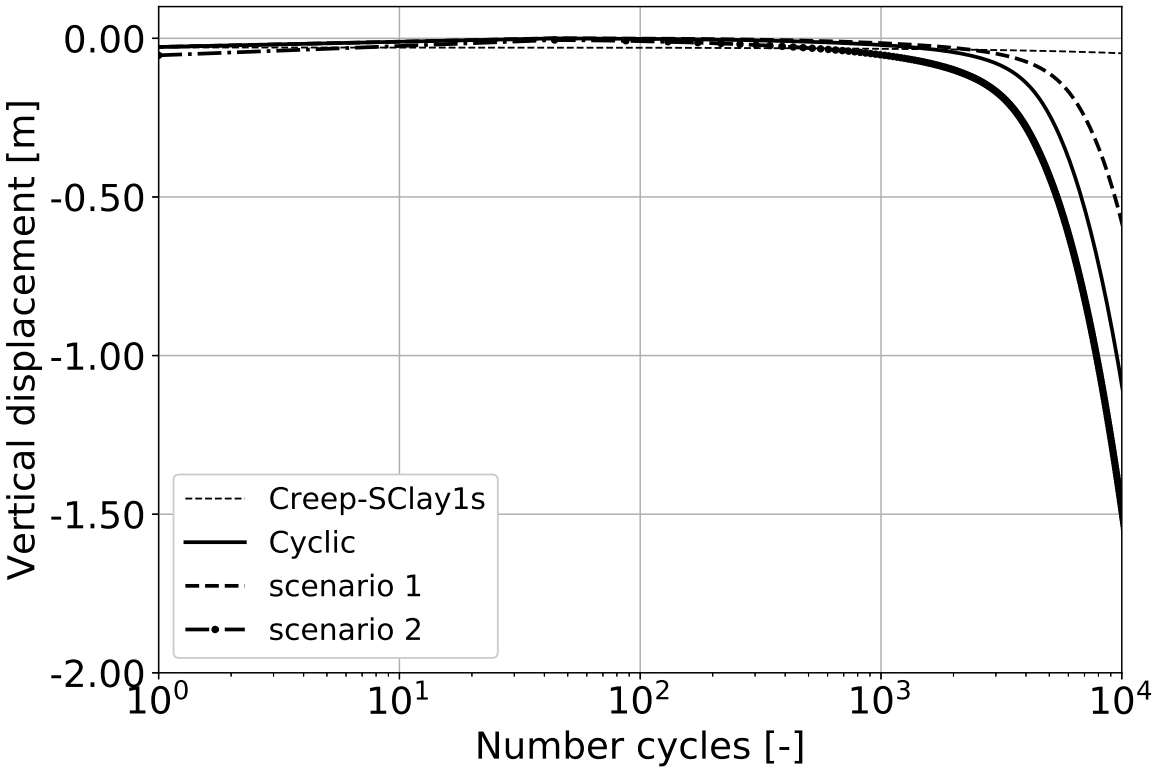


Figure 12: Vertical displacement of the point located along the axis of symmetry at the interface between the embankment and the soil.

Appendix B - Paper on sensitivity analysis

Computers and Geotechnics 90 (2017) 164–175

Contents lists available at ScienceDirect

Computers and Geotechnics

journal homepage: www.elsevier.com/locate/compgeo

Research Paper

Strategy for consistent model parameter calibration for soft soils using multi-objective optimisation

J.-P. Gras [a], N. Sivasithamparam [b], M. Karstunen [a], J. Dijkstra [a,*]

[a] Chalmers University of Technology, Department of Civil and Environmental Engineering, SE-412 96 Gothenburg, Sweden
[b] Norwegian Geotechnical Institute, P.O. Box 3930, Ullevål Stadion, N-0806 Oslo, Norway

ARTICLE INFO

Article history:
Received 13 November 2016
Received in revised form 8 May 2017
Accepted 7 June 2017
Available online 23 June 2017

Keywords:
Soft soil
CREEP-SCLAY1S
Sensitivity analysis
Multi-objective optimisation

ABSTRACT

Constitutive models for soft soils require a large number of parameters to model the complex material response. One set of parameters should capture the soil response for various laboratory & in situ stress paths. This requires a new method to calibrate a consistent set of model parameters using test data from different load paths of classic geomechanical tests. The feasibility of the proposed method is demonstrated with the recently developed CREEP-SCLAY1S model. After a sensitivity analysis that highlights the model parameters for optimisation, an optimisation process for two different configurations is designed. The latter is successfully verified against artificially generated laboratory data.

© 2017 Elsevier Ltd. All rights reserved.

1. Introduction

Soft clays are very complex materials. Advanced models taking into account anisotropy, time/rate dependency, bonding/destructuration and non-linear elasticity are required to correctly describe and predict their mechanical behaviour. An unfortunate side effect is that these advanced models require a large number of parameters. Generally, in such models, most of these parameters are directly assessed from a single type of laboratory test, but some cannot be measured experimentally. It is then necessary to estimate these parameters through indirect methods such as calibration [1].

Automatic methods for model calibration are essential in order to identify model parameters independently of the user. Often these methods are based on the inverse problem theory by [2]. It consists of finding the best set of parameters which minimises the distance between experimental results and model results. Numerous methods for inverse analysis for geotechnical problems have been carried out with gradient methods [3–6], neural network based techniques [7,8], genetic algorithms [9,10] and particle swarm optimisation [11–13].

Generally, the parameter identification techniques based on inverse analysis remain unsatisfactory because they do not sufficiently take into account the non-uniqueness of the inverse analysis problems. This difficulty can be overcome by determining a set of satisfactory solutions (multi-objective optimisation process) or the use of several test types with different load paths [14]. The difficulty to obtain the uniqueness of the solution is increasing with the number of parameters to optimise. Practically, it is not feasible to obtain all parameter values for complex models with many parameters. There is then a need to choose the proper parameters for optimisation. Principally, the optimisation parameters are only the parameters which are not measurable experimentally. However, even the parameters that are directly derived from experimental data have some measurement uncertainties which will affect the final output.

In this article, the uniqueness of the solution is studied using artificial data. The optimisation method uses a genetic algorithm combined with selected relevant test paths to obtain reliable model parameter solutions. In order to choose the parameters for optimisation, a sensitivity analysis was performed for different test paths with a different set of model parameters and initial conditions. From the sensitivity analysis, the most important parameters, which need to be optimised, are identified.

2. Software framework

An overview of the principle work flow of the software tool is shown in Fig. 1. Three important stages are highlighted in grey. Two of those, i.e. the sensitivity analysis and optimisation of

* Corresponding author.
E-mail addresses: jean-philippe.gras@chalmers.se (J.-P. Gras), nallathamby.siva@ngi.no (N. Sivasithamparam), minna.karstunen@chalmers.se (M. Karstunen), jelke.dijkstra@chalmers.se (J. Dijkstra).

http://dx.doi.org/10.1016/j.compgeo.2017.06.006
0266-352X/© 2017 Elsevier Ltd. All rights reserved.

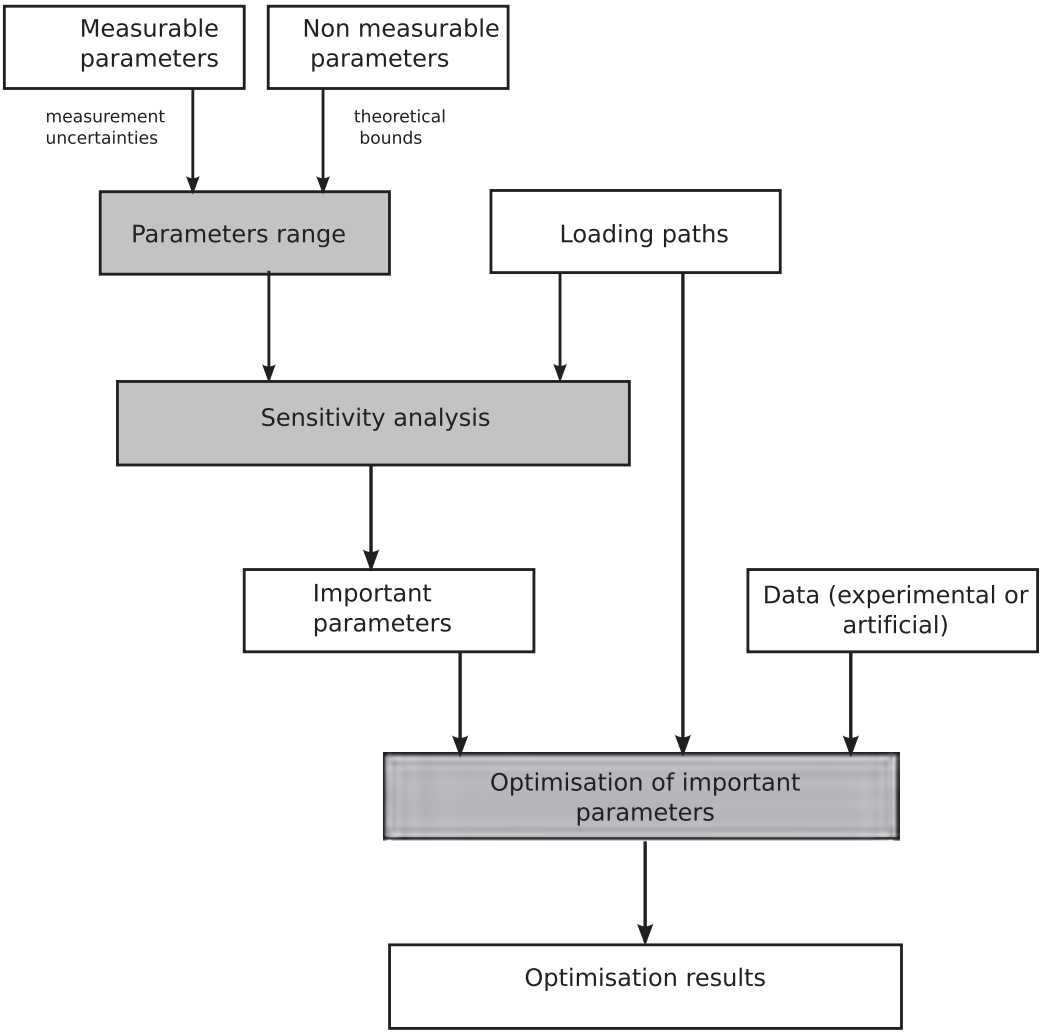


Fig. 1. Flow chart of the optimisation method.

parameters, are implemented as two modules in the tool. In contrast the third, the selection of the parameter bounds, is limited by the model formulation and potential measurement errors and requires further user input as is elaborated in [15].

The software tool is in fact a graphical user interface (GUI) wrapped around an incremental driver, developed by [16,17], using the Python PyQt library. The incremental driver enables probing the constitutive model on a single integration point level for arbitrary stress and strain paths and is compatible with the syntax of the user-defined material subroutine of ABAQUS, i.e. UMAT. The implementation is universal where the Python code calls the incremental driver, which is a standalone executable, see Fig. 2. In principle any constitutive model implemented as a UMAT library can be linked to the incremental driver, and hence the Python wrapper. Furthermore, this enables straightforward expansion towards parallelisation with multiple threads, each one calling an incremental driver. In the current implementation the number of loading paths that can be evaluated is limited by the available test data rather than computational limitations.

The Python GUI allows for easy access to additional libraries for sensitivity analyses and model optimisation. The sensitivity analysis tool to study the importance and sensitivity of parameters of the constitutive model in the strain driver is implemented using the Sensitivity Analysis Library, the SALib package [18]. The optimisation tool, to optimise model parameters against experimental data, has been implemented via the Distributed Evolutionary Algorithms in Python, DEAP, library [19]. Both tools may be used for one loading path or multiple loading paths.

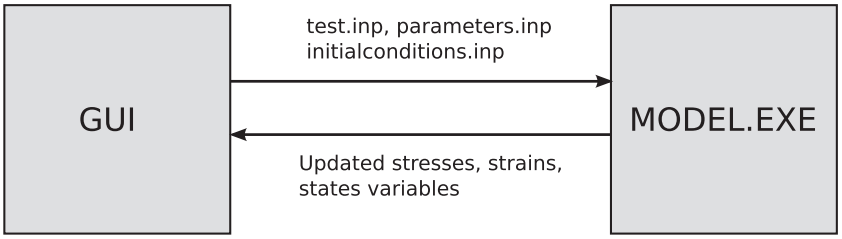


Fig. 2. Communication between the Graphical User Interface (GUI) wrapper script and the incremental driver.

Although the tools are universal and in principle any constitutive model can be used, it is recommended to use a model that in its basis has sufficient capabilities. An overly simple model, such as e.g. Mohr Coulomb, is unable to capture the stress-strain curve of any laboratory test. Furthermore, in principle, the model parameters are easily derived from the laboratory test at hand (but perhaps not consistent for different test types). Instead the presented methodology is aimed at obtaining a consistent model parameter set for an advanced hardening model that is able to capture a wide range of loading paths.

3. Parameters and load tests

In this section, the model parameters are briefly described as well as the three different sets of parameters used for the studies (sensitivity and optimisation analysis). The loading cases used for these two analyses are also presented.

3.1. Description of the parameters

The Creep-SCLAY1S model is developed for slightly overconsolidated or normally consolidated soft clays. The Creep-SCLAY1S model requires 14 model parameters divided into 11 soil constants: the modified swelling index κ^*, the Poisson's ratio for unloading/reloading ν', the intrinsic parameter related to irrecoverable compression ξ_i^*, the slope of critical state line in compression M_c, the slope of critical state line in extension M_e, the intrinsic modified creep index μ_i^*, the reference time τ, the absolute effectiveness of rotational hardening ω, the relative effectiveness of rotational hardening ω_d, the absolute rate of destructuration a, the relative rate of destructuration b, and three initial state variables: the stress ratio corresponding to a normally consolidated state K_0^{nc}, the initial preconsolidation pressure σ_{p0}, the initial inclination of the reference surface α_0 and the initial amount of bonding χ_0 (see Appendix for more details on model parameters).

The reference time τ is known (controlled during the laboratory test) so that there is no uncertainty for this parameter, therefore τ will not be considered in the further analysis. K_0^{nc} will not be considered either as it is directly evaluated from the simplified Jaky's formulae [20], as well as ω_d which can be directly evaluated based on the formulation of the model (see Appendix). The definition of the measured parameters and their derivation are presented in the Appendix, as well as some considerations about bounds for K_0^{nc} and the effect of this parameter on the model. For other parameters, more information is available in [15].

From a literature review, minimum and maximum values for the measurable parameters are presented in Table 1, as well as their assumed measurement uncertainties. For σ_{p0}, there is not a range, as it depends largely on the depth of the soil sample and sample quality. For the optimisation and sensitivity analysis, three different sets of parameters are used and presented in Table 3 (Set 1, Set 2 & Set 3).

3.2. Description of load tests

Sensitivity analyses are performed for five different load paths from classical geomechnical tests: Anisotropically Consolidated Drained test in Compression (CADC) or Extension (CADE), Anisotropically Consolidated Undrained test in Compression (CAUC) or Extension (CAUE) and so-called 1D Constant Rate of Strain test (CRS). Optimisation is performed only on CRS, CAUC and CAUE. For the two triaxial drained tests (CADC and CADE), q and $\varepsilon_v = \varepsilon_{vert} + 2\varepsilon_{lat}$ are the output variables meanwhile for the two triaxial undrained tests (CAUC and CAUE) these are p' and q. For the CRS test, the variables of interest are σ'_{vert} and σ'_{lat}. For all these strain controlled tests, the abscissa considered is the time t. The displacement rate, the strain rate and the final strain applied in each test simulation are as follows:

- 0.001 mm/min or 1.44%/day for the drained triaxial tests. The final axial strain is 15% for the CADC and 10% for the CADE.
- 0.01 mm/min or 14.4%/day for the undrained triaxial tests. The final axial strain is 5%.
- 0.0024 mm/min or 17%/day for the CRS tests. The final axial strain is 30%.

The initial vertical effective stresses are respectively 46 kPa, 100 kPa and 50 kPa for Sets 1, 2 and 3. The initial horizontal effective stresses are respectively equal to 28 kPa, 60 kPa and 26 kPa for the Sets 1, 2 and 3. The shear stresses are equal to zero for all tests. In the CRS test simulations, the initial stress conditions are different with vertical and horizontal effective stresses equal to 5 kPa. The load tests are plotted in Fig. 3.

4. Sensitivity and uncertainty analysis

First a brief overview of the method used is presented. Then the results of the sensitivity analyses are discussed, and the important parameters which needs optimisation are highlighted.

4.1. Description of the method

A sensitivity analysis is used first to rank model parameters by their importance or their sensitivity regarding to different mechanical load paths. For analysis of the influence of the parameter on the output, a distinction is made between uncertainty analysis (parameter importance) and sensitivity analysis (parameter sensitivity) [21]. An 'important' parameter will be a parameter the uncertainty of which contributes substantially to the uncertainty in the results,

Table 1
Description of the minimum and maximum values for measurable parameters, their assumed values of measurement uncertainties and the three parameter sets used for the study.

Parameters	Min - Max	$\Delta error\%$	Set 1	Set 2	Set 3
$\kappa^*(*10^{-2})$	0.7–4.4	20	2.5	1.5	3.5
ν'	0.10–0.35	20	0.20	0.20	0.20
$\xi_i^*(*10^{-2})$	1.5–25	10	6.00	9.80	5.60
M_c	0.8–1.7	5	1.30	1.50	1.67
M_e	0.6–1.1	5	0.90	1.10	1.07
σ_{p0}	-	20	61	115	65
χ_0	5–100	20	20	4.0	13.0
$\mu_i^*(*10^{-3})$	0.1–6	20	1.5	3.0	1.40
ω	-	-	33	14	30
α_0	-	-	0.42	0.58	0.67
a	-	-	10.0	8.0	12.5
b	-	-	0.40	0.20	0.35

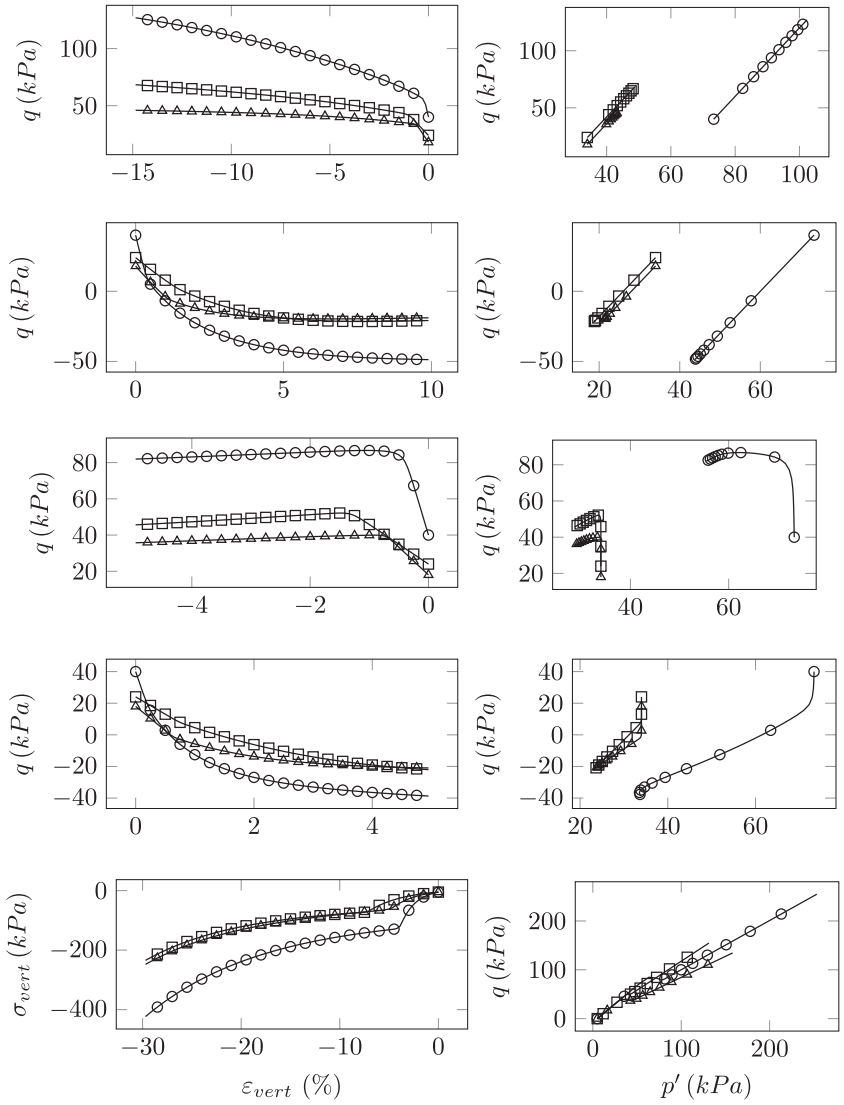


Fig. 3. From the first row to the fifth row, the output of the model for the CADC, CADE, CAUC, CAUE and CRS test are plotted. The triangle, circle and square markers, respectively refer to the Set 1, 2 and 3 of parameters with associated initial stresses conditions.

meanwhile a 'sensitive' parameter will be parameter highly correlated with the model output so that small changes in the input values may result in significant changes in the output of the model. One should notice, that a sensitive parameter is not necessarily an important parameter because it may be known precisely. For this reason, two different ranges of uncertainties are used for the sensitivity analysis:

- Range 1: 10% of uncertainties is applied for all parameters in order to investigate qualitatively which parameters are the most correlated with the output (the most 'sensitive').
- Range 2: This range takes into account the assumed measurement uncertainties summarized in Table 1. The bounds used for non measurable parameters such as α_0, w, a and b are derived from theoretical considerations in [15]. This range will provide quantitatively the most 'important' parameters for a real case based on best estimates for the measured uncertainties. Range 2 is also the range used for the optimisation process.

For more details on the values used for the range, see the Appendix.

The Sobol method [22–26], implemented using the SALib package [18], is used. The Sobol method is a variance-based measure, which is reliant on decomposing the variance of the output. Variance based methods are well suited to take parameters interactions into account. In order to look at the total influence of the input parameters on the output, we are interested in the total effect index S_T [27,28], which is a measure of first and higher effects (interactions) of parameters. The total effect index S_T measures the contribution to the output variance of one parameter, including all variance caused by its interactions, of any order, with any other input parameters. Contrary to the Morris method [29], which is used mostly to sort the parameter by their relative influence on the output, the Sobol method allows for an accurate quantification of the sensitivity.

In this study, the outputs are not single constant values but evolving variables following a given loading path. To define the output of our model as a scalar value, an error function is used which defines the difference between the modelled and the reference behaviour. For one particular variable Y_j, the error function $F^j_{err}(X)$ is defined by:

$$F^j_{err}(X) = \frac{1}{N}\left[\sum_{i=1}^{N}\left|\frac{A^i_{ref} - A^i_{sol}(X)}{A^i_{ref}}\right|^2\right]^{\frac{1}{2}} \quad (1)$$

X is the vector of input parameters, $A^i_{sol}(X)$ is ith interval area of the model curve of the variable Y_j for a given X, A^i_{ref} is the ith interval area of reference (in general, it corresponds to a set of parameters with the nominal values), N is the number of intervals used to discretise the data (see Fig. 4). In this study, the abscissa is the time. The error function is made independent of the measurement interval and minimised for steep gradients by considering the area [14]. In case of n different variables $Y_1, \ldots, Y_j, \ldots, Y_n$ with a single scalar output, the following error function $F_{err}(X)$ is used to define the scalar value output of our model:

$$F_{err}(X) = \frac{1}{n}\left[\sum_{j=1}^{n} F^j_{err}(X)\right] \tag{2}$$

This error function is used in the sensitivity analysis to investigate the effect of changing parameters X on the difference between model outcome and the reference data. The same error function is used for the optimisation process. For the sensitivity analysis presented next, a single scalar output is used for each load test (n = 1). For the optimisation, two (CRS, CAUC) or three load tests (CRS, CAUC, CAUE) are used to calculate the error function.

4.2. Results of the analysis

The results from the Sobol method for the five different load paths and two different ranges are plotted in Fig. 5. On this Figure, the mean result value of the three different sets is plotted. Then, for each loading path, the parameters are ranked from the most sensitive/important to the least sensitive/important in Table 2. Interestingly, for all loading paths and both ranges, χ_0 and μ^*_i have a negligible effect on the model output.

Fig. 5 shows the results for Range 1 and Range 2 for the five different load tests. Firstly, the results corresponding to Range 1 are discussed. σ_{p0} is a very sensitive parameter for all loading paths. For extension tests (CADE and CAUE), similar trends are observed with $\sigma_{p0}, M_e, M_c, \kappa^*, \nu', \alpha_0$ and w as the most sensitive. Interestingly, ω, which controls the rate of rotation of the stress surface, is not as sensitive as the other parameters. For compression tests (CADC, CAUC and CRS), similar trends are observed with $\sigma_{p0}, M_c, \xi^*_i$ as the most sensitive parameters. a is relatively important in CADC and CRS tests whereas α_0 is quite important for the CAUC test. It is interesting that ξ^*_i is the most sensitive parameter in the CRS tests, where κ^* is also quite sensitive. The structure parameters such as χ_0, a and b have negligible influence for undrained tests, but have some influence in the drained tests. This is due to the low strain levels considered (5%) with only limited destructuration. Similar trends are observed for Range 1 and Range 2 where in most cases the most sensitive parameters are also the most important, only the ranking differs. There are some notable differences, however:

- ω is an important parameter in the extension tests (Fig. 5A and C). This is partly due to the fact that this parameter has a big uncertainty range and partly due to large degree of fabric rearrangement in such loading path.
- a and b are more influential for Range 2, notably in compression tests (Fig. 5B and D). a has a small impact for undrained tests with no volumetric strain ε_v, hence overall b has a bigger impact.
- ξ^*_i is not the most important parameter in the CRS loading path. It was the most sensitive regarding Range 1. This is due to smaller measurement uncertainties.
- M_c or M_e are not very important parameters, as they may be measured rather accurately in the laboratory and are independent of any sample destructuration. M_c has still some importance in the CADC tests.

Finally, $\kappa^*, \nu', \xi^*_i, \sigma_{p0}, \omega, \alpha_0, a$ and b are important parameters and may require further optimisation or an improvement on the measurement accuracy (for the measurable parameters). For example, the measurement of ξ^*_i and ν' may be improved with high quality tests on high quality samples. The other parameters seem to have no importance for the measurement accuracy of Range 2, it is then possible to fix them. Considering the results on different load paths, the number of optimised parameters will also depend on the engineering problem. When compression behaviour is dominant, the parameters related to anisotropy and its evolution, ω and α_0, may not be needed to be optimised. If, on the other hand, compression and extension paths are equally important, more parameters need to be considered for optimisation (or measured accurately). K^{nc}_0 may be important as well when it is included as a separate parameter (see Appendix).

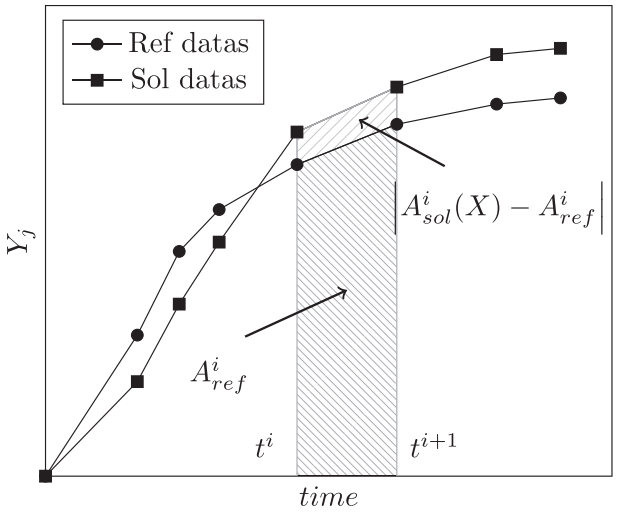


Fig. 4. Illustration of the calculus of $F^i_{err}(X)$ corresponding to variable Y_j. On each interval, the area between the two curves $A^i_{sol}(X) - A^i_{ref}$ is divided by the area of the reference data A^i_{ref}. This figure is an illustration for the ith interval.

5. Optimisation

First, an overview of the Genetic Algorithms is presented. Then, the non-uniqueness of the solution is highlighted with an example. Finally, a method is proposed to obtain the desired parameters from the optimisation, and the results are discussed.

5.1. Genetic algorithm description

Genetic Algorithms are originally developed by [30]. In a genetic algorithm, a population of individuals is evolved towards better solutions of an optimisation problem. Each individual contains genes (here parameters of the model). The evolution starts from a population of randomly generated individuals and evolve towards a population with reduced value of the fitness of each individual. The fitness is the value of the objective function (in this study, it is defined by the error function presented in Eq. (2)). Each iteration is called a generation. The population evolves using a combination of selection, crossover and mutation operators specific to each genetic algorithm. The crossover operator is an operator which allows individuals to share their genes. The mutation operator allows a mutation of the genes of the individual (values of some parameter may change occasionally from one generation to other). The selection process which selects the individuals for the next

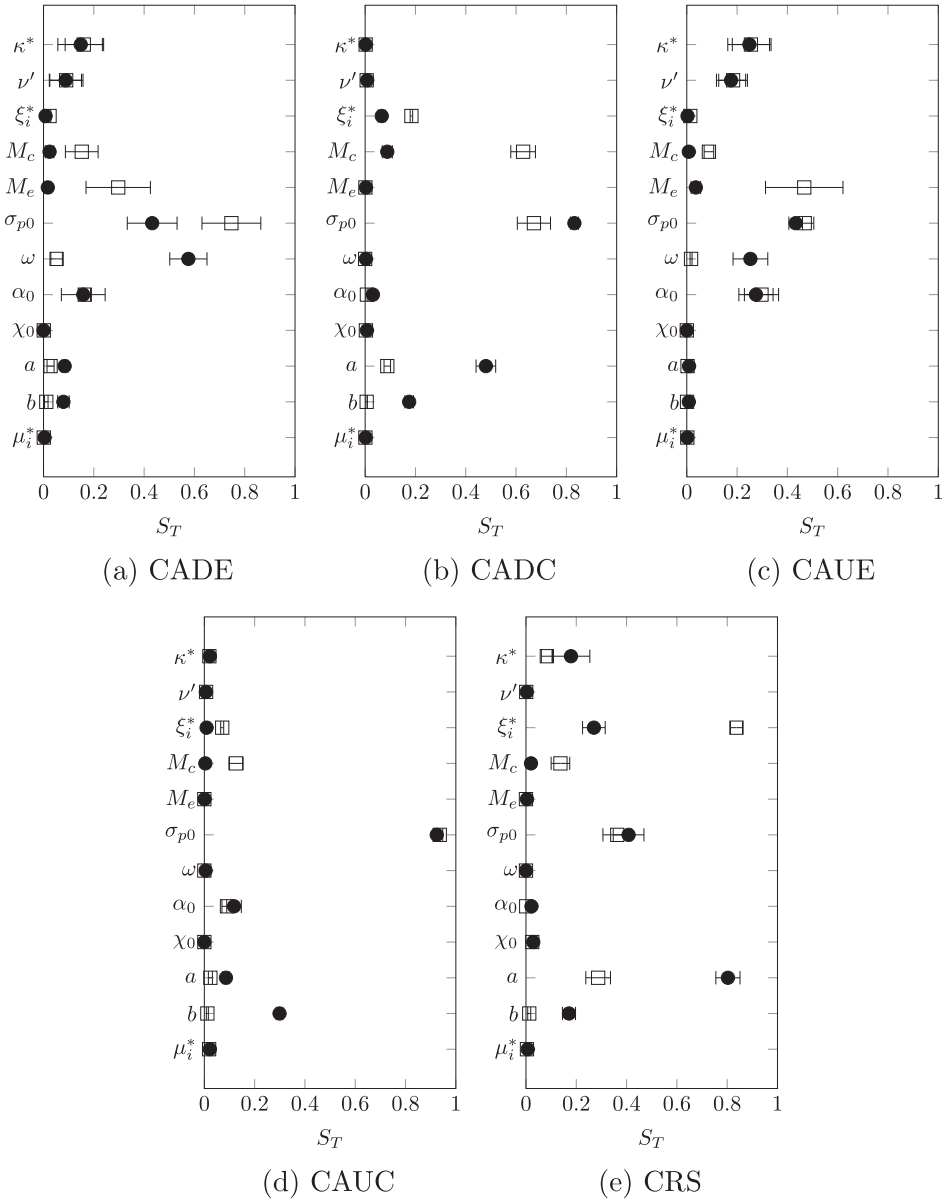


Fig. 5. Results of the sensitivity analysis for different loading paths with two ranges of uncertainties. Range 1 and Range 2 are, respectively, represented by solid circle and empty square.

Table 2
Most sensitive and most important parameters ranked by their order of importance for different loading paths.

Loading Path	Range 1: most sensitive	Range 2: most important
CADE	$\sigma_{p0}, M_e, M_c, \kappa^*, \nu', \alpha_0, \omega$	$\omega, \sigma_{p0}, \alpha_0, \kappa^*, \nu', a, b$
CADC	$\sigma_{p0}, M_c, \xi_i^*, a$	$\sigma_{p0}, a, b, M_c, \xi_i^*$
CRS	$\xi_i^*, \sigma_{p0}, a, M_c, \kappa^*$	$a, \sigma_{p0}, \xi_i^*, b, \kappa^*$
CAUE	$\sigma_{p0}, M_e, \alpha_0, \kappa^*, \nu', M_c$	$\sigma_{p0}, \alpha_0, \omega, \kappa^*, \nu'$
CAUC	$\sigma_{p0}, M_c, \xi_i^*, \alpha_0$	$\sigma_{p0}, b, \alpha_0, a$

generation is often based on the fitness value. Commonly, the algorithm terminates when, either a maximum number of generations has been produced, or a satisfactory fitness level has been reached for the population. For the optimisation process, a modified version [31] of the popular NSGA-II genetic algorithm [32] is used and implemented via the Deap library [19]. This alternative formulation prevents premature convergence in comparison to the previous versions providing additional diversity. This algorithm is a non-dominated multi-objective algorithm, which works reasonably well up to two or three objective functions. This algorithm is also suited for mono-objective optimisation problems [33].

5.2. Difficulties in optimisation

One difficulty when dealing with optimisation of several parameters is to find a unique set of parameters. When the number of parameters to be optimised n is larger than the number of output variables m, a unique solution for the parameters is impossible.

The parameters $\kappa^*, \nu', \xi_i^*, a, b, \sigma_{p0}, \omega$ and α_0 were optimised against reference data of q and p' as a function of time t from a single CAUC test. Range 2 of parameters is used for the optimisation process. The reference data was created from the model using a set of reference parameters X_{ref} (Set 1). The initial horizontal and vertical effective stress were, respectively, 28 kPa and 46 kPa. Two cases were considered. In Case 1, the reference data was exactly the generated artificial data from the model. In Case 2, 5%

Table 3
Description of the three different parameter sets and their range used in the sensitivity analysis and optimisation.

Parameters	Set 1		Set 2		Set 3	
	Range 1	Range 2	Range 1	Range 2	Range 1	Range 2
$\kappa^*(*10^{-2})$	2.25–2.75	2.0–3.0	1.35–1.65	1.20–1.80	3.15–3.85	2.80–4.20
ν'	0.18–0.22	0.16–0.24	0.18–0.22	0.16–0.24	0.18–0.22	0.16–0.24
$\xi_i^*(*10^{-2})$	5.40–6.60	5.40–6.60	8.82–10.78	8.82–10.78	5.04–6.16	5.04–6.16
M_c	1.17–1.43	1.23–1.36	1.35–1.65	1.42–1.57	1.50–1.84	1.58–1.75
M_e	0.81–0.99	0.85–0.94	0.99–1.21	1.04–1.15	0.96–1.18	1.06–1.12
σ_{p0}	54.9–67.1	48.8–73.2	104–127	105–138	58.5–71.5	55.0–78.0
χ_0	18–22	16–24	3.6–4.4	3.2–4.8	11.7–14.3	10.4–15.6
$\mu_i^*(*10^{-3})$	1.35–1.65	1.20–1.80	2.7–3.3	2.4–3.6	1.26–1.54	1.12–1.68
ω	29.7–36.3	1–40	12.6–15.4	1–28	27–33	1–44
α_0	0.38–0.46	0.37–0.52	0.52–0.64	0.43–0.62	0.60–0.74	0.50–0.72
a	9.0–11.0	4.8–19.6	7.2–8.8	3.5–14.8	11.3–13.8	5.3–21.7
b	0.36–0.44	0–1	0.18–0.22	0–1	0.32–0.39	0–1

random noise is added to the reference data to better reflect non-perfect experimental data. This noise amplitude represents the largest scatter encountered in a typical laboratory test. Scatter in-between laboratory tests due to e.g. heterogeneity, sample disturbance will be partly mitigated by the mono-objective multi-objective optimisation process as all tests have some sensitivity to most parameters. For each case, nine different optimisation processes were performed resulting in nine different set of parameters solution. The evolution of q and p' as a function of t simulated with these nine sets of parameters is plotted in Fig. 6b for smooth data and in Fig. 6d for noisy data. The curves simulated with the optimisation parameters are very close to the reference data with errors less than 0.05% for smooth data and less than 1.67% for noisy data. In Fig. 6a and c, nine curves are plotted (corresponding to the nine different sets of parameter solutions, respectively, for smooth data and noisy data) to represent the relative variation $\left(\frac{X_{opt}-X_{ref}}{X_{ref}}(\%)\right)$ of each parameter solution X_{opt} from its corresponding reference parameter X_{ref} . Clearly, the set of parameter solutions is non-unique, meanwhile the error between the model with optimisation parameters X_{opt} and with reference parameters X_{ref} is very small. For some parameters, such as σ_{p0}, α_0 or ξ_i^* the optimisation results are quite similar when comparing different runs, whereas for parameters a, b or ω the results present some disparities. These results corroborate the sensitivity analysis, and it is quite logical that the most sensitive parameter for this test (CAUC test) are predicted best. Fig. 6a and c, clearly show that a, b and ξ_i^*, which are parameters related to the size of the reference surface, are highly correlated. Notably, in Fig. 6a and c, the smaller the value a, the bigger the value b and ξ_i^*, and the bigger is a, the smaller are b and ξ_i^*. The combination of these three variables seems more important than their individual values, highlighting a possible inconsistency in the model.

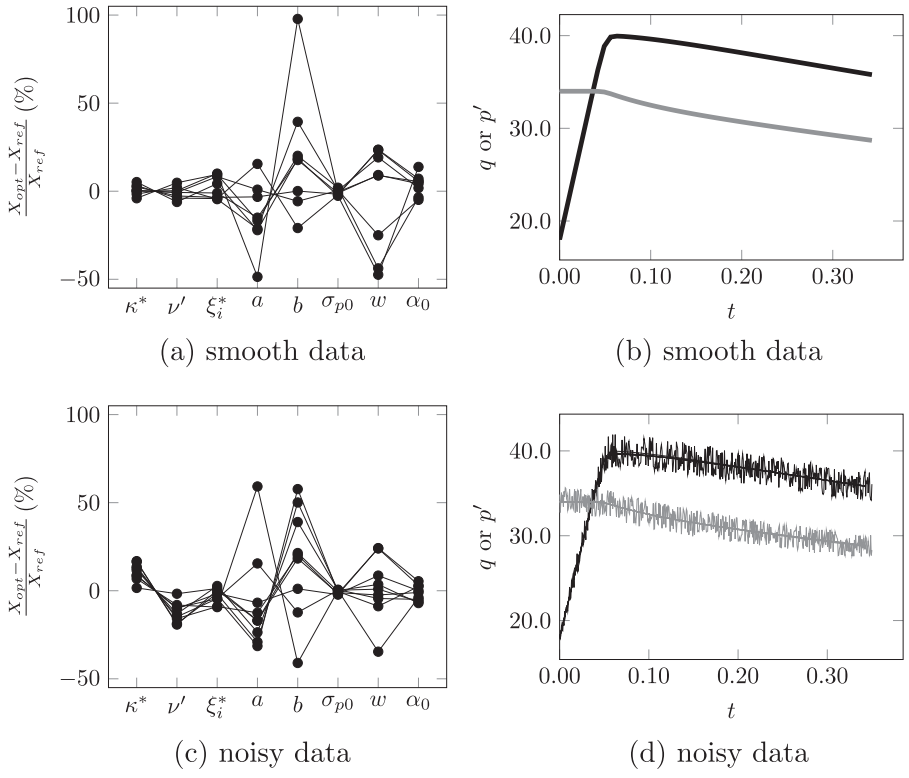


Fig. 6. Subplots (a) and (c) represent the variability of the parameter solution for nine different optimisation runs for smooth and noisy data, respectively. In subplots (b) and (d), the reference data and the simulated data corresponding to the nine parameter sets solution for the CAUC test are plotted. The evolution of p' and q are, respectively, plotted in gray and dark gray.

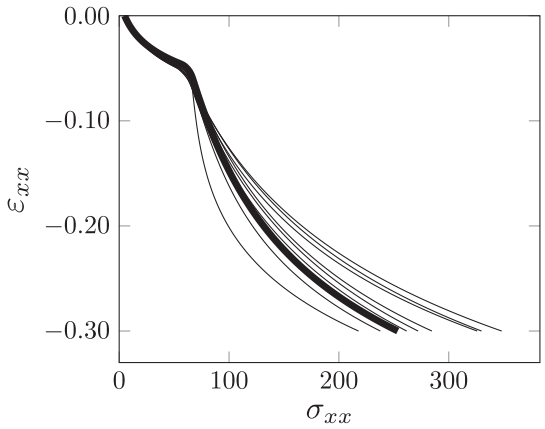


Fig. 7. Model output for the CRS test using the nine optimized parameter set solutions of the CAUC test.

When comparing the results of the model using previous optimised parameters X_{opt} and reference parameters X_{ref} for a different loading path (CRS test), however, it becomes obvious that the results are not anymore similar (see Fig. 7). Parameters a and b that are sensitive parameters for the CRS test were not so sensitive for the CAUC test. Therefore, a method is proposed to optimise the important parameters using the most appropriate load paths.

5.3. Design of the optimisation process

For the optimisation of a, b, ξ_i^*, it seems appropriate to include the CRS test for which these parameters are more sensitive. For ω and α_0, and ν' a triaxial extension test is required. A CRS test or triaxial extension test is appropriate for κ^*. σ_{p0} is sensitive for most tests. Two different configurations were studied:

1 Optimisation for loading in compression and extension by optimising $\sigma_{p0}, \xi_i^*, \kappa^*, \nu', a, b, \omega$ and α_0. K_0^{nc} may be adjusted or optimised if there is poor agreement with Jaky's relation. The optimisation of these parameters is conducted by comparing model data to reference data from CRS, CAUC and CAUE tests. These represent five different variable measurements: σ_{xx} (vertical effective stress) for CRS and q and p' for CAUC and CAUE tests.
2 Optimisation for mainly compressive load paths, optimising $\sigma_{p0}, \xi_i^*, \kappa^*, a$ and b. Again K_0^{nc} might be adjusted if deemed necessary. The optimisation of these parameters is conducted by comparing model data to reference data from CRS and CAUC tests. These incorporate three different variable measurements: σ_{xx} for CRS and q and p' for CAUC tests.

In both cases the optimisation process compares the model with clean and noisy artificial data (5% random noise superimposed). The number of parameters to optimise is larger than the number of measurements or error functions, hence a unique solution is unattainable. More tests would give a better definition of the parameters, however, from a practical point of view that would increase the optimisation time and reduce the applicability in engineering practice. No drained triaxial tests are considered here, as these tests are rarely conducted for soft soils.

5.4. Results of optimisation

First of all, it is noted that the optimisation process converges. For both configurations, the error function is very small with less than 1.7% of error for noisy data (which is less than the 5% added noise amplitude) and less than 0.5% for smooth data. Variability of the parameter solution for different configuration and noisy and smooth reference data are presented in Fig. 8. Generally, it seems quite surprising that adding noise reduces the variability of the parameter solution, except for parameters κ^* and ν', which were more stable with smooth data. For Configuration 1, taking

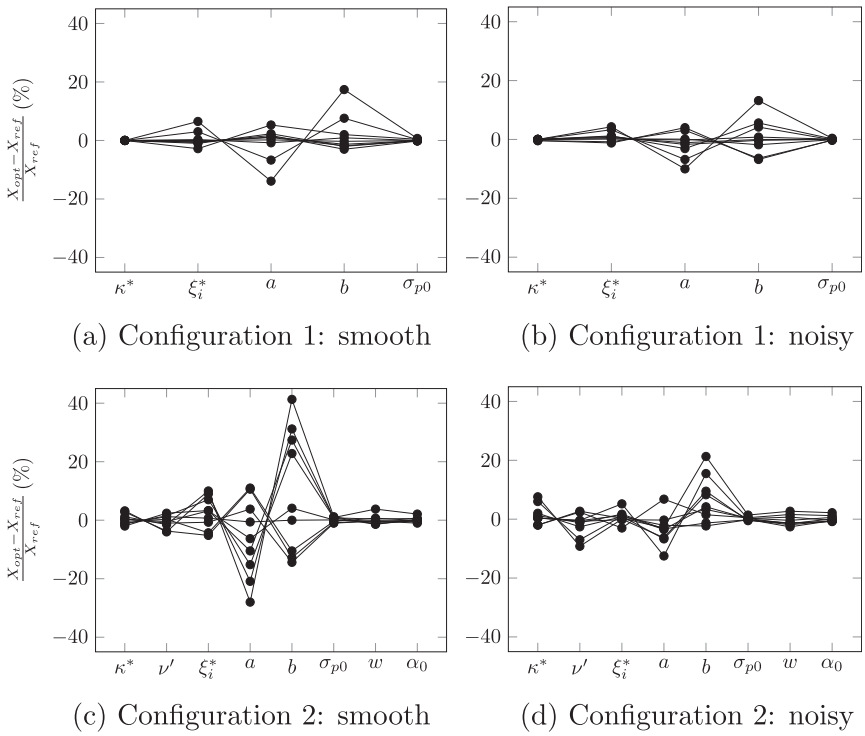


Fig. 8. Variability of the parameter solution for nine different optimization run for Configuration 1 & 2 with smooth and noisy data.

into account the extension path, eight parameters were optimised: $\sigma_{p0}, \xi_i^*, \kappa^*, \nu', a, b, \omega$ and α_0. It is observed that the values obtained for $\sigma_{p0}, \kappa^*, \nu', \omega$ and α_0 are quite stable with optimised values close to the reference data. Concerning, ξ_i^*, a and b, much more variation from the reference values is observed.

Configuration 2 shows similar results, where the five following parameters were optimised: κ^*, ξ_i^*, a, b and σ_{p0}. The values obtained for κ^* and σ_{p0} are very close to the reference values for all tests. This time values for ξ_i^*, a and b show more variation. Fig. 8 clearly shows that these three variables related to the evolution of the size of the reference surface are highly correlated. When ξ_i^* is large, a is small and b is large. For the paths tested, the combination of these three variables is more important than each single value. One possibility is to consider ξ_i^* as a fitting parameter, but in that case issues could probably arise when all the structure is erased and no effect from a and b is present.

In both configurations it would be best to run several optimisation processes, and to keep the ones with the lowest error function, as for those, the optimisation parameters are the closest to the reference set of parameters. One solution may also be to measure ξ_i^* with more accuracy and hence not having to optimise it.

6. Conclusions

A new comprehensive toolkit is introduced where a generic software wrapper, written in Python, is used to run an incremental driver originally developed by [17]. The incremental driver allows for testing arbitrary strain and stress paths for any constitutive model implemented in UMAT format. The wrapper implements the sensitivity and optimisation libraries so that (i) the important and sensitive model parameters as function of loading path can be identified for (ii) further optimisation (calibration) using mono-objective or multi-objective optimisation against laboratory data. Furthermore, it is demonstrated for a complex non-linear model with 14 parameters that this procedure is successful using only a limited number of loading paths that are easily obtained from standard element level laboratory tests. Simulations with artificial data, both with and without added noise that simulates the maximum experienced uncertainties in laboratory data, demonstrate the robustness of the method. The expectation is that the method will work well with real data.

First, the assessment of the most important parameters of a complex rate-dependent model for natural soft clays is made, using two types of sensitivity analyses for different classical geotechnical tests (CADC, CADE, CAUC, CAUE, CRS). These sensitivity analyses used three different parameter sets (with typical values for soft clays), and initial stress conditions. All these analyses show similar trends highlighting the most important parameters for each test (i.e. loading path). Based on this analyses, certain parameters were identified to be the most important parameters for design involving both loading paths in compression and extension representing e.g. deep excavations and deep foundations (Configuration 1) and a subset of these parameters were identified to be the most important parameters for design mainly involving loading paths in compression such as embankments (Configuration 2). The optimisation, using a genetic algorithm, was ran using three different geomechanical tests to optimise parameters for Configuration 1 (CAUE, CAUC and CRS), and two tests to optimise parameters of Configuration 2 (CAUC and CRS). The optimisation was performed by comparing the model data with artificial data sets in order to verify the optimisation procedure. Both optimisation processes converge well with error functions less than 0.5%. Some parameters are very stable and very close to the real values of parameters, however, three model parameters presented some disparities, indicating high correlation between these three parameters, identifying a potential shortcoming in the model formulation. If the best solutions of multiple runs are, however, selected the original values for these interdependent parameters are retrieved with sufficient accuracy. Consequently, it is suggested to execute several optimisation runs and keep the one with the lowest error function.

Acknowledgements

The research was carried out as part of CREEP (Creep of Geomaterials, PIAP-GA-2011–286397) project supported by the European Community through the programme Marie Curie Industry-Academia Partnerships and Pathways (IAPP) under the 7th Framework Programme. Furthermore, the financial support from Trafikverket in the framework Branch samverkan i Grund (BIG) is greatly acknowledged. JD is supported by a Fellowship grant EC/FP7-MC-IEF 623613 EMPIRIC.

Appendix A

A.1. Anisotropy parameter ω_d

ω_d is related to the relative effectiveness of rotational hardening expressed by [34]:

$$w_d = \frac{3\left(4M_c^2 - 4\eta_{K_0^{nc}}^2 - 3\eta_{K_0^{nc}}\right)}{8\left(\eta_{K_0^{nc}}^2 - M_c^2 + 2\eta_{K_0^{nc}}\right)} \tag{3}$$

where $\eta_{K_0^{nc}}$ is the value of stress ratio corresponding to a normally consolidated value of K_0^{nc}. $\eta_{K_0^{nc}} = 3(1 - K_0^{nc})/(1 + 2K_0^{nc})$. Here, this derived value of ω_d is used in the model and consequently ω_d is eliminated as input parameter.

A.2. Elastic parameters κ^* and ν'

The modified swelling index κ^* is the slope of the $\epsilon_v^e - \ln p'$ curve in the elastic domain, with p' the mean effective stress. κ^* may vary for sensitive clays, but for modelling purposes, its largest value may be used [35] in order to be conservative. In practice, the isotropic modified swelling index κ^* is often calculated from the one dimensional swelling index C_s measured in the $e - \log \sigma'_{vert}$ plane during oedometer tests assuming K_0 equal to 1 and ν' equal to 0.2:

$$\kappa^* \approx \frac{2}{2.3}\frac{C_s}{(1 + e_0)} \tag{4}$$

As the one-dimensional unloading is not at constant stress ratio, the link between C_s and κ^* is not so obvious [36]. Then if κ^* is derived from such a test will have a lot of uncertainties. It is also important to notice that κ^* presents an unloading/re-loading hysteresis. In that case a choice needs to be made corresponding to the problem we are dealing with.

ν', the Poisson's ratio for elastic unloading/reloading, is assumed to be constant.

A.3. Compressibility parameter ξ_i^*

ξ_i^* is equal to $\lambda_i^* - \kappa^*$ and is an intrinsic parameter related to irrecoverable compression. λ_i^*, the modified intrinsic compression index, is the slope of the intrinsic compression line in $\varepsilon_v - \ln p'$ plane (see Fig. 9). It can be measured from re-constituted soil samples or for undisturbed samples at (very) high stresses (assuming all the bonds are erased for high stresses). λ_i^* could also be assessed from the slope of the intrinsic compression line in $e - \log \sigma'_a$ plot

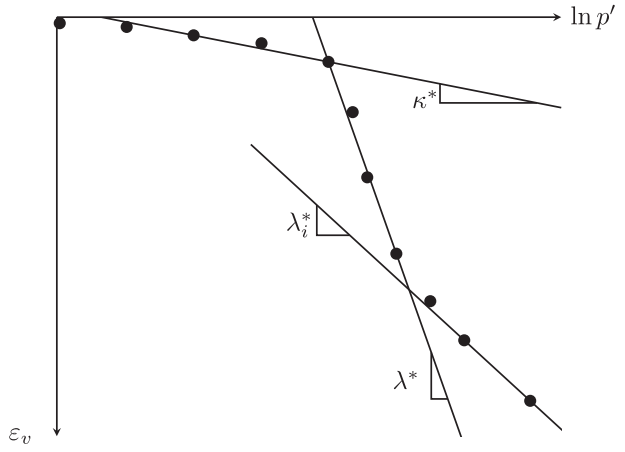


Fig. 9. Definition of λ^*, λ_i^* and κ^*.

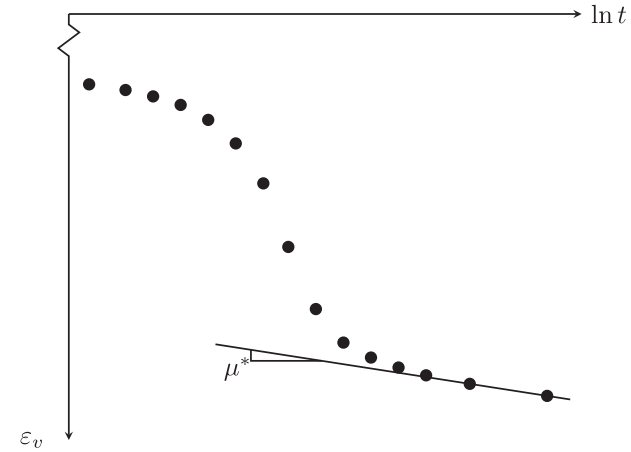


Fig. 10. Definition of μ^*. For high value of stress or for reconstitued sample, when all the structure is erased, $\mu^* \to \mu_i^*$.

usually called the intrinsic compression index C_{ci}. The relation between λ_i^* and C_{ci} is:

$$\lambda_i^* = \frac{C_{ci}}{2.3(1+e_0)} \tag{5}$$

A.4. Critical state parameters M_c and M_e

A Lode angle formulation is used to differentiate between the critical state line in triaxial extension M_e and in triaxial compression M_c. Both are the ratio between the deviator stress $q = (\sigma_{vert} - \sigma_{lat})$ and the effective mean stress $p' = 1./3.(\sigma'_{vert} + 2\sigma'_{lat})$ when critical state is reached in a triaxial test following, respectively, an extension or compression loading path. For high quality test execution on natural samples, it is estimated that the experimental assessed values have uncertainties in the order of 5%.

A.5. The vertical pre-consolidation pressure σ_{p0}

The vertical pre-consolidation pressure σ_{p0} is required to determine the initial size of the Normal Compression Surface (NCS), representing the boundary of small and large irrecoverable strains. The experimental assessment of the pre-consolidation pressure is generally made in the semi-logarithmic plane (void ratio - $\log \sigma_{vert}$). It is assumed that the value measured experimentally has an uncertainty of 20%.

A.6. Creep parameters μ_i^* and τ

Considering 1D oedometer conditions, the volumetric creep strain rate $\dot{\epsilon}_v$ is given by a power law as follows:

$$\dot{\epsilon}_v = \frac{\mu_i^*}{\tau}\left(\frac{p'_{eq}}{p'_p}\right)^{\beta} \tag{6}$$

μ_i^*, the intrinsic modified creep index, is the slope of the curve in the $\epsilon_v - \ln t$ plane, after the end of the consolidation process (see Fig. 10). It is an intrinsic parameter, i.e. it should be derived from data where all the structure is erased (for large values of stress or tests on reconstituted soil samples). μ_i^* is the limit value of the slope of the curve in the $\epsilon_v - \ln t$ when t is increasing (see Fig. 10). It could be also derived from the intrinsic secondary compression index $C_{\alpha i}, C_{\alpha i} = \Delta e / \Delta \log t$, by:

$$\mu_i^* = \frac{C_{\alpha i}}{2.3(1+e_0)} \tag{7}$$

There is a high probability that the real value of μ_i^* is smaller than the value derived from experimental data. Indeed, we are not sure to have attained the intrinsic state completely, and sometimes the slope of the curve in the $\epsilon_v - \ln t$ is still decreasing at the end of the test.

The reference time is the duration of the load step in the oedometer test used to obtain the initial pre-consolidation pressure. For example, if the initial normally pre-consolidation pressure is derived from a standard oedometer test loaded with 24 h load steps, the reference time τ is set to one day [37]. Then, given appropriate test execution, the value of τ is known with high precision and does not need optimisation or sensitivity analysis. The value of μ_i^* should be derived using the same time unit as for the description of the reference time τ.

A.7. Structure/bonding parameters χ_0

As a first approximation, the value of the initial bounding χ_0 may be derived from the sensitivity S_t as follows [38]:

$$\chi_0 = S_t - 1 \tag{8}$$

The sensitivity of a soil, i.e. the ratio between the undisturbed peak strength between and the remoulded strength can be measured in several ways: field or laboratory vane, Swedish fall-cone test.

A.8. The stress ratio corresponding to a normally consolidated state K_0^{nc}

K_0^{nc} can be deduced from the simplified Jaky's formula [20]:

$$K_0^{nc} = 1 - \sin\varphi' \tag{9}$$

where the friction angle φ' at critical state is related to M_c using $M_c = 6\sin\varphi'/(3-\sin\varphi')$ using the Mohr-Coulomb failure envelope. In that case, K_0^{nc} is not an additional optimisation parameter, as it is directly derived from the value of M_c. K_0^{nc} can also be an additional parameter if Jaky's relation gives unsatisfactory results. From Eq. (3), $\eta_{K_0^{nc}}$ should stay in the following range to avoid negative or undetermined values for w_d:

$$-\frac{3-\sqrt{9+64M_c^2}}{8} < \eta_{K_0^{nc}} < \frac{-2+\sqrt{4+4M_c^2}}{2} \tag{10}$$

Bounds for K_0^{nc} are then directly related to $\eta_{K_0^{nc}}$ bounds and plotted in Fig. 11a. In that case, adjusting K_0^{nc} will have two effects on the output of Creep-SCLAY1S:

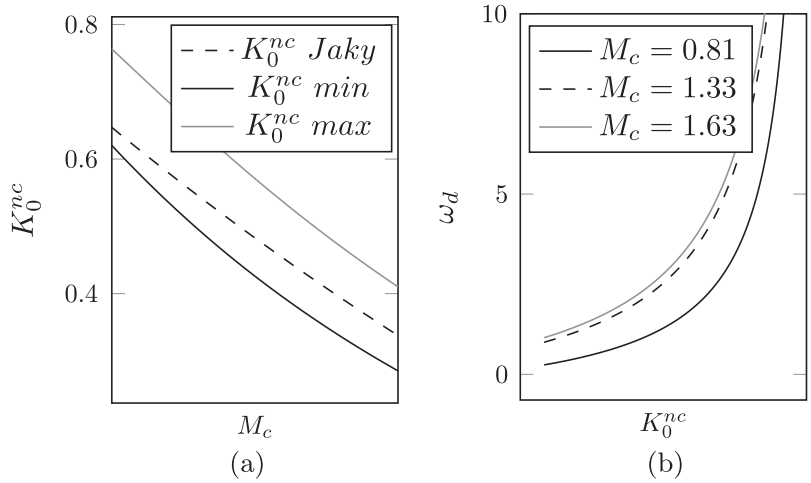


Fig. 11. (a):Bounds for K_0^{nc} as a function of M_c (M_c varies from 0.8 to 1.6). (b): w_d as a function of K_0^{nc} (K_0^{nc} varies from K_0^{nc} *Jaky* to almost K_0^{nc} *max*) for different values of M_c.

- It will change the value of the initial isotropic pre-consolidation pressure p_m,
- It will affect the relative importance of creep deviatoric strains on the rotation of the stress surface by modifying w_d (Eq. (3)). Indeed, if K_0^{nc} is calculated from Jaky's formula, w_d remains in a range between 0.5 and 2 for M_c in the range 0.8–1.63, but if K_0^{nc} increases w_d increases (see Fig. 11b) and will have a larger influence on the rotation of the surfaces. It would be interesting to check the importance of this parameter, for example for an undrained extension test where significant rotation is expected due to plastic (creep) deviatoric strains.

A.9. Ranges used for optimisation and sensitivity process values for the three set of parameters

The values of the range used for the three sets of parameters for the optimisation and sensitivity analysis are presented in Table 1.

References

[1] Vrugt J, Gupta H, Bastidas L, Bouten W, Sorooshian S. Effective and efficient algorithm for multiobjective optimization of hydrologic models. Water Resour Res, vol. 39, 8.

[2] Tarantola A. Inverse problem theory and methods for model parameter estimation. SIAM; 2005.

[3] Anandarajah A, Agarwal D. Computer-aided calibration of a soil plasticity model. Int J Numer Anal Methods Geomech 1991;15(12):835–56.

[4] Calvello M, Finno R. Selecting parameters to optimize in model calibration by inverse analysis. Comput Geotech 2004;31(5):410–24.

[5] Dano C, Hicher P-Y, Rangeard D, Marchina P. Interpretation of dilatometer tests in a heavy oil reservoir. Int J Numer Anal Methods Geomech 2007;31 (10):1197–215.

[6] Ledesma A, Gens A, Alonso E. Estimation of parameters in geotechnical backanalysis I. Maximum likelihood approach. Comput Geotech 1996;18 (1):1–27.

[7] Obrzud R, Vulliet L, Truty A. A combined neural network/gradient-based approach for the identification of constitutive model parameters using self-boring pressure meter tests. Int J Numer Anal Methods Geomech 2009;33 (6):817–49.

[8] Hashash Y, Jung S, Ghaboussi J. Numerical implementation of a neural network based material model in finite element analysis. Int J Numer Methods Eng 2004;59(7):989–1005.

[9] Levasseur S, Malécot Y, Boulon M, Flavigny E. Soil parameter identification using a genetic algorithm. Int J Numer Anal Methods Geomech 2008;32 (2):189–213.

[10] Taborda D, Pedro A, Coelho P, Antunes D. Impact of input data on soil model calibration using genetic algorithms. Numerical Methods in Geotechnical Engineering:(NUMGE 2010); 2000, vol. 69.

[11] Meier J, Schaedler W, Borgatti L, Corsini A, Schanz T. Inverse parameter identification technique using PSO algorithm applied to geotechnical modeling. J Artif Evol Appl 2008;2008:3.

[12] M. Fontan, A. Ndiaye, D. Breysse, P. Castéra, Inverse Analysis in Civil Engineering: Applications to Identification of Parameters and Design of Structural Material Using Mono Or Multi-objective Particle Swarm Optimization, 2012, pp. 87–114 [ch 6].

[13] Ye L, Jin Y-F, Shen S-L, Sun P, Zhou C. An efficient parameter identification procedure for soft sensitive clays. J Zhejiang Univ Sci A 2016;17(1):76–88.

[14] Papon A, Riou Y, Dano C, Hicher P-Y. Single-and multi-objective genetic algorithm optimization for identifying soil parameters. Int J Numer Anal Methods Geomech 2012;36(5):597–618.

[15] Gras JP, Sivasithamparam N, Karstunen M, Dijkstra J. Permissible range of model parameters for natural fine-grained materials. Acta Geotech. doi:http://dx.doi.org/10.1007/s11440-017-0553-1.

[16] Gudehus G, Amorosi A, Gens A, Herle I, Kolymbas D, Mašín D, Muir Wood D, Niemunis A, Nova R, Pastor M. The soilmodels.info project. Int J Numer Anal Methods Geomech 2008;32(12):1571–2.

[17] Niemunis A. Incremental driver. User's manual, University of Karlsruhe KIT; 2008.

[18] Herman J, Usher W. SALib: An open-source Python library for sensitivity analysis. Journal of Open Source Softw 2017;2(9). http://dx.doi.org/10.21105/joss.00097.

[19] Fortin F-A, De Rainville F-M, Gardner M, Parizeau M, Gagné C. DEAP: evolutionary algorithms made easy. J Mach Learn Res 2012;13:2171–5.

[20] Jaky J. The coefficient of earth pressure at rest. J Soc Hungar Arch Eng 1944;78 (22):355–8.

[21] Hamby D. A review of techniques for parameter sensitivity analysis of environmental models. Environ Monitor Assess 1994;32(2):135–54.

[22] Sobol I. On sensitivity estimation for nonlinear mathematical models. Mate Model 1990;2(1):112–8.

[23] Saltelli A, Chan K, Scott EM. Sensitivity analysis, vol. 1. New York: Wiley; 2000.

[24] Makowski D, Naud C, Jeuffroy M-H, Barbottin A, Monod H. Global sensitivity analysis for calculating the contribution of genetic parameters to the variance of crop model prediction. Reliab Eng Syst Saf 2006;91(10):1142–7.

[25] Cariboni J, Gatelli D, Liska R, Saltelli A. The role of sensitivity analysis in ecological modelling. Ecol Model 2007;203(1):167–82.

[26] Saltelli A, Ratto M, Andres T, Campolongo F, Cariboni J, Gatelli D, Saisana M, Tarantola S, et al. Global sensitivity analysis: the primer. John Wiley & Sons; 2008.

[27] Homma T, Saltelli A. Importance measures in global sensitivity analysis of nonlinear models. Reliab Eng Syst Saf 1996;52(1):1–17.

[28] Saltelli A, Tarantola S, Chan K. A role for sensitivity analysis in presenting the results from MCDA studies to decision makers. J Multicriteria Decis Anal 1999;8(3):139.

[29] Morris M. Factorial sampling plans for preliminary computational experiments. Technometrics 1991;33(2):161–74.

[30] Holland J. Adaptation in natural and artificial systems: an introductory analysis with applications to biology, control, and artificial intelligence. U Michigan Press; 1975.

[31] Fortin F-A, Parizeau M. Revisiting the nsga-ii crowding-distance computation. In: Proceedings of the 15th annual conference on genetic and evolutionary computation. ACM; 2013. p. 623–30.

[32] Deb K, Pratap A, Agarwal S, Meyarivan T. A fast and elitist multiobjective genetic algorithm: NSGA-II. IEEE Trans Evol Comput 2002;6(2):182–97.

[33] Seada H, Deb K. U-nsga-III: a unified evolutionary optimization procedure for single, multiple, and many objectives: proof-of-principle results. In: Evolutionary multi-criterion optimization. Springer; 2015. p. 34–49.

[34] Wheeler S, Näätänen A, Karstunen M, Lojander M. An anisotropic elastoplastic model for soft clays. Canad Geotech J 2003;40(2):403–18.

[35] Sivasithamparam N, Karstunen M, Bonnier P. Modelling creep behaviour of anisotropic soft soils. Comput Geotech 2015;69:46–57.
[36] Wood DM, Mackenzie N, Chan A. Selection of parameters for numerical predictions. In: Predictive soil mechanics: proceedings of the wroth memorial symposium, Oxford, UK. London: Thomas Telford; 1992. p. 496–512.
[37] Leoni M, Karstunen M, Vermeer P. Anisotropic creep model for soft soils. Géotechnique 2008;58(3):215–26.
[38] Koskinen M, Zentar R, Karstunen M. Anisotropy of reconstituted poko clay. In: Proceedings of the 8th international symposium in numerical models in geomechanics (NUMOG); 2002. p. 99–105.

BIG – Branschsamverkan i grunden
Forskningsprogram för effektiv och säker grundläggning av vägar och järnvägar

BIG

BIG – Branschsamverkan i grunden - är ett forskningsprogram för effektiv och säker grundläggning av transportsystemets infrastruktur. Programmet etablerades under senhösten 2013, och påbörjade sin verksamhet den 1 januari, 2014.

Målsättningen är att sänka kostnader för byggande och underhåll av transportsystemets infrastruktur genom ett långsiktigt och systematiskt utvecklingsarbete inom geoteknikområdet.

I BIG samverkar Trafikverket, Chalmers tekniska högskola, Luleå tekniska universitet, Kungliga tekniska högskolan och Statens geotekniska institut.

Resultat från BIG projekt publiceras i vetenskapliga artiklar och parternas egna rapportserier. Alternativt så publiceras rapporterna i denna gemensamma BIG rapport serie.

Publicerade rapporter

A2014:03	Deformationer i undergrund – Litteratursammanställning och analys
A2014:07	Grundvattensänkning i morän
A2014:13	Höghastighetsspår i Sverige – på bank
A2014:14	On the fundamental relation between soil creep and cyclic pile-soil response
A2017:10	Effects of climate change on slopes in sensitive clay
A2016:05	Modelling deformations below high-speed rail